# Fire safety of facades

*BRĂNIȘTEANU-ALBULESCU Bogdan-Grigore*

**Fire Safety Engineering**

**Lund University**

**Sweden**

**Report 5589, Lund 2019**

**Master Thesis in Fire Safety Engineering**

FIRE SAFETY OF FACADES

BRĂNIȘTEANU-ALBULESCU Bogdan-Grigore

Report 5589
ISRN: LUTVDG/TVBB—5589—SE

Number of pages: 73
Illustrations: 61

Keywords
polystyrene, graphene, façade, pyrolysis

Abstract
Façade fires are a big concern due to past incidents and the large number of victims encountered. Vertical flame spread mechanism specific to this type of fires is a complex phenomenon with parameters that are often difficult to be coupled. Moreover, the architectural design of the façade assemblies further complicates the evaluation of the fire safety strategies.
The energy reduction requirements have led to an increased use of combustible insulating materials. Polystyrene is one of the first synthetic polymers used on a large scale for thermal insulation of the buildings. Due to its remarkable properties like transparency, high chemical stability and dielectric qualities it is the most preferred material among plastics. Although, polystyrene is a combustible material, it is still used on the construction market due to its highly insulating properties. Often designers need to make a compromise in the early stage of the building to achieve a balance between fire safety strategies and the energy reduction requirements. Since these requirements are strongly interrelated there is a continuous need for further improvement of the construction materials used for facades.
The main goal of this thesis is to quantitatively evaluate the flammability properties of different polystyrene compounds and to investigate whether the addition of graphene in their composition could enhance these properties.
The experimental measurements using graphene PS masterbatch have shown important improvements in the fire properties of the polystyrene compound. The interaction between graphene and polystyrene matrix generates changes during the chemical reaction of this thermoplastic material.
Numerical simulations using Fire Dynamics Simulator have been performed in order to validate the accuracy of the pyrolysis model embedded into this CFD package on one hand and to qualitatively compare the temperatures recorded during an external fire which replicates the testing conditions presented by BS 8414 procedure, on the other. Heat release rate curves obtained for the Microscale Combustion Calorimeter (MCC) numerical simulations, offered encouraging results as their shape closely follows the experimental studies.



---

Fire Safety Engineering

Lund University

P.O. Box 118

SE-221 00 Lund

Sweden

**DISCLAIMER**

This thesis is submitted in partial fulfilment of the requirements for the degree of *The International Master of Science in Fire Safety Engineering (IMFSE)*. This thesis has never been submitted for any degree or examination to any other University/programme. The author declares that this thesis is an original work, except where stated. This declaration constitutes an assertion that full and accurate references and citations have been included for all material, directly included and indirectly contributing to the thesis. The author gives permission to make this master thesis available for consultation and to copy parts of this master thesis for personal use. In the case of any other use, the limitations of the copyright have to be respected, in particular with regard to the obligation to state expressly the source when quoting results from this master thesis. The thesis supervisor must be informed when data or results are used.

Read and approved,

BRĂNIȘTEANU-ALBULESCU Bogdan-Grigore

30.04.2019

## Abstract

Façade fires are a big concern due to past incidents and the large number of victims encountered. Vertical flame spread mechanism specific to this type of fires is a complex phenomenon with parameters that are often difficult to be coupled. Moreover, the architectural design of the façade assemblies further complicates the evaluation of the fire safety strategies.

The energy reduction requirements have led to an increased use of combustible insulating materials. Polystyrene is one of the first synthetic polymers used on a large scale for thermal insulation of the buildings. Due to its remarkable properties like transparency, high chemical stability and dielectric qualities it is the most preferred material among plastics. Although, polystyrene is a combustible material, it is still used on the construction market due to its highly insulating properties. Often designers need to make a compromise in the early stage of the building to achieve a balance between fire safety strategies and the energy reduction requirements. Since these requirements are strongly interrelated there is a continuous need for further improvement of the construction materials used for facades.

The main goal of this thesis is to quantitatively evaluate the flammability properties of different polystyrene compounds and to investigate whether the addition of graphene in their composition could enhance these properties.

The experimental measurements using graphene PS masterbatch have shown important improvements in the fire properties of the polystyrene compound. The interaction between graphene and polystyrene matrix generates changes during the chemical reaction of this thermoplastic material.

Numerical simulations using Fire Dynamics Simulator have been performed in order to validate the accuracy of the pyrolysis model embedded into this CFD package on one hand and to qualitatively compare the temperatures recorded during an external fire which replicates the testing conditions presented by BS 8414 procedure, on the other. Heat release rate curves obtained for the Microscale Combustion Calorimeter (MCC) numerical simulations, offered encouraging results as their shape closely follows the experimental studies.

## Abstract (Romanian)

Incendiile pe fațadele clădirilor sunt un motiv de îngrijorare datorită evenimentelor din trecut și a numărului mare de victime rezultate în urma acestora. Mecanismul de propagare pe verticală, specific acestui tip de incendii, reprezintă un fenomen complex cu parametri ce adesea sunt foarte dificil de evaluat. În plus, proiectarea din punct de vedere architectural al sistemelor de fațadă complică și mai mult evaluarea măsurilor de securitate la incendiu.

Cerințele privind reducerea consumului de energie au condus la creșterea utilizării materialelor combustibile termoizolante. Polistirenul este unul din primii polimeri sintetici utilizați pe scară largă la izolarea termică a clădirilor. Datorită proprietăților sale remarcabile precum transparența, stabilitate chimică ridicată și a comportamentului dielectric, este cel mai utilizat material din categoria plasticului. Deși polistirenul este un material combustibil, el este încă utilizat pe piața construcțiilor datorită proprietăților sale de izolare termică. Astfel, adesea proiectanții sunt obligați să realizeze un compromis încă din stadiul inițial al construcției pentru a obține un echilibru între securitatea la incendiu și cerințele privind reducerea consumului de energie. Deoarece aceste cerințe sunt strâns corelate între ele, există un continuu interes pentru îmbunătățirea materialelor de construcție utilizate pentru izolarea termică a fațadelor.

Principalul obiectiv al acestei teze este de a evalua din punct de vedere cantitativ proprietățile de combustibilitate ale diferitelor produse pe bază de polistiren și de a cerceta dacă prin introducerea grafenului în compoziția acestora proprietățile menționate pot fi îmbunătățite.

Studiile experimentale utilizând peleți de polistiren cu grafen au arătat modificări importante în ceea ce privește combustibilitatea polistirenului. Interacțiunea dintre grafen și structura polistirenului generează schimbări pe timpul reacțiilor chimice suferite de acest material termoplastic.

Modelarea matematică utilizând Fire Dynamics Simulator a avut ca scop determinarea modului în care modulul de piroliză inclus în acest program de tip CFD oferă rezultate corecte pe de o parte, precum și pentru a compara calitativ temperaturile dezvoltate pe timpul unui incendiu exterior ce reproduce condițiile de testare stabilite de către standardul BS 8414. Curbele specifice ratei de căldură degajată obținute prin simularea matematică a microcalorimetrului (MCC) oferă rezultate încurajatoare având în vedere că forma acestora reproduce încercările experimentale.

## Acknowledgments

This thesis report was done during the last semester of the International Master of Science in Fire Safety Engineering program at Lund University, under the coordination of prof. dr. Patrick van Hees, the Head of Division of Fire Safety Engineering.

First of all, I would like to thank my supervisor for giving me the opportunity to work on this interesting topic. He is the one who supported my ideas from the first stage of the work and continuously offered me valuable guidance on the progress of this research.

I am grateful to Frank Markert, Associate Professor at Technical University of Denmark, who granted me access to the testing facilities and helped me to run measurements with their Bomb Calorimeter and TGA-DSC apparatus. I am also grateful to Jens Steeman Kristensen, PhD candidate at The University of Edinburgh, who is currently located at Technical University of Denmark, for giving me the technical advice and support throughout the Bomb Calorimeter experiments.

I am thankful to Lars Wadsö, Professor at Division of Building Materials at Lund University, for his thoroughly induction on Transient Plane Source usage and also for his valuable advice related to the data analysis.

Credits to Bjarne Paulsen Husted, Senior lecturer at Division of Fire Safety Engineering at Lund University, for his invaluable inputs on the CFD simulations and for the technical IT support, which proved to be critical for the achievement of the final report.

Special thanks are going to Dan Madsen, Lecturer at Division of Fire Safety Engineering at Lund University, who actively helped me to perform the measurements and provided the experimental results. Thank you for your patience during the entire semester and for your professional approach that gave me the possibility to fulfill each task.

I appreciate all the efforts of the IMFSE coordinators, secretary and colleagues for creating such an interesting and multinational group, without which this work would not have been possible.

Last but not least, I would like to thank my family and my wife, Victoria, for their financial and moral support throughout the entire program.

## Table of contents

## NOMENCLATURE

BR – BUILDING REGULATIONS

BS – BRITISH STANDARD

CAN/ULC – CANADIAN STANDARD

CFD – COMPUTATIONAL FLUID DYNAMICS

DIN – GERMAN STANDARD

DSC – DIFFERENTIAL SCANNING CALORIMETRY

EIFS – EXTERNAL INSULATION FAÇADE SYSTEMS

EN – EUROPEAN STANDARD

EPS – EXPANDED POLYSTYRENE

ETAG – EUROPEAN APPROVAL TECHNICAL GUIDELINES

ETICS – EXTERNAL THERMAL INSULATION COMPOSITE SYSTEM

FDS – FIRE DYNAMICS SIMULATOR

GO – GRAPHENE OXIDE

HPL – HIGH PRESSURE LAMINATES

HRR – HEAT RELEASE RATE

ISO – INTERNATIONAL STANDARD ORGANIZATION

LDPE – LOW-DENSITY POLYETHYLENE

MCC – MICROSCALE COMBUSTION CALORIMETER

MCM – METAL COMPOSITE CLADDING

OSB – ORIENTED STRAND BOARD

PMMA – POLYMETHYL METHACRYLATE

PS - POLYSTYRENE

SP – SWEDISH NATIONAL TESTING AND RESEARCH INSTITUTE (now RISE)

SIPS – STRUCTURAL INSULATION PANEL SYSTEMS

TGA – THERMOGRAVIMETRIC ANALYSIS

TPS – TRANSIENT PLANE SOURCE

XPS – EXTRUDED POLYSTYRENE

## List of figures

## List of tables

# 1. INTRODUCTION

## 1.1 Motivation and objectives

In a world confronting environmental challenges, there is a fervent requirement for dynamic building envelopes that respond to climatic changes in an ideal way, thereby giving the best comfort and indoor environmental quality, while keeping up high effectiveness.

New innovative insulating materials for facades can provide step-change upgrades in the energy efficiency and the use of renewable energy while improving the comfort inside the buildings for their occupants. Due to the energy reduction and efficiency requirements, the thermal rehabilitation of the existing buildings has grown up in the recent years across Europe. Thus, one of the most accessible and cost-effective technical solution to achieve this desiderate is represented by the external insulation with expanded polystyrene slabs.

Polystyrene is one of the first synthetic polymers used on a large scale for thermal insulation of the buildings. Due to its remarkable properties like transparency, high chemical stability and dielectric qualities it is the most preferred material among plastics.

Like any other organic polymers, polystyrene is burning, having a melting point around $240^0$ C and an ignition temperature close to $427^0$C [1]. Since it is a combustible material it contributes to a rapid fire spread over facades leading to disastrous consequences involving loss of human life and property damage.

At this moment, there are two types of polystyrene on the construction market with enhanced fire properties. To begin with, graphite-polymer nanocomposites are used to increase thermal stability and mechanical properties of the material, as well. The graphite structure consists of carbon layers in an alternating stacking sequence. The carbon atoms are bounded covalently in a hexagonal arrangement within the layer and these layers are weakly bounded to each other. Secondly, different fire retardant substances are injected in the chemical structure of the insulator in order to improve fire performance properties of the construction material.

Although, polystyrene is a combustible material, it is still used on the construction market due to its highly insulating properties. Often designers need to make a compromise in the early stage of the building to achieve a balance between fire safety strategies and the energy reduction requirements. Since these requirements are strongly interrelated there is a continuous need for further improvement of the construction materials used for facades.

One way to deal with this issue would be to develop new materials that can fulfill these requirements, or at least to be on an acceptable range for both fields. One of the goals of the proposed thesis is to evaluate a new polystyrene-based material using graphene properties. From 2004 when graphene was for the first time discovered, many research activities were performed in order to develop various methods for its production. One of the most promising methods for large scale production of graphene is by chemical oxidation

exfoliation of graphite leading to graphene oxide. The incorporation of small amount of graphene into polymers can achieve substantial enhancement in properties like reinforcement, damage tolerance, electrical and thermal conductivity, corrosion protection and flame retardancy [2].

According to Yue et al. [3] the thermal degradation of the expanded polystyrene occurs in two steps, first at 153 °C and then at 385 °C. Compared with polystyrene matrix, the graphene composite shows a single decomposition platform at 385 °C. Graphene polystyrene specimen displays improved thermal stability properties as indicated by a delayed onset of degradation in comparison to expanded polystyrene, as shown in figure 1. The thermal decomposition temperature of graphene polystyrene nanocomposite is higher than that of expanded polystyrene, indicated that there was a strong interaction between graphene oxide sheets and polystyrene matrix. There is a clear evidence that the incorporation of graphene oxide has led to important improvement in thermal stability of the polystyrene matrix. The improvement in thermal stability may be due to the high heat capacity and thermal conductivity of graphene oxide. Besides, the interfacial interactions between graphene oxide and polystyrene can lead to the formation of physical or chemical cross-linking points which hinder the degradation of polystyrene chains to a certain extent. Furthermore, the graphene oxide plates that cover the polystyrene particles provide a barrier to the escape of volatiles from polymer decomposition and decrease the mass loss [3].

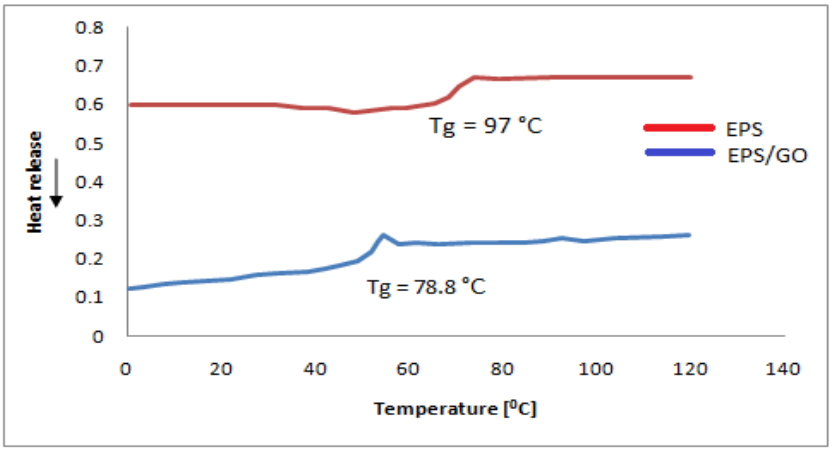


Figure 1 Heat release for graphene polystyrene (redrawn from [3])

The overall combustibility and the reaction-to-fire performances of the façade systems could be enhanced by replacing the traditional insulating materials with more versatile and less combustible products. The above research results have led to an important improvement in the heat release of the graphene polystyrene compounds which further encourages a more in depth approach for the determination of the flammability and combustibility capabilities of this material.

As the performance-based design methods using a computational approach are often involved in the design stage of the buildings, the evaluation of the accuracy and the

reliability of the CFD packages has become an interesting topic among researchers. Although Fire Dynamics Simulator has been proven to be a useful tool in the fire safety engineering field, it has still numerous drawbacks that need further improvement. The pysolysis models included in the FDS are a first step in the numerical modeling of the spread of flames over the combustible materials. The validation of this model could generate a better understanding of this pending problem, in the same time strengthening the reliability of the CFD packages.

The main objectives of this thesis are:

- to determine and calculate different flammability parameters using experimental results;
- to assess the fire characteristics of the polystyrene compounds used for the thermal insulation of the external building facades;
- to determine the input parameters for FDS pyrolysis simulation;
- to better understand the fire behavior of polystyrene-based materials and to qualitatively describe their characteristics.

The first step of the present research which addresses the first three objectives of this study would be focused on testing experiments on the raw material. Properties like kinetic reaction parameters, heat of reaction, heat of combustion and heat capacity need to be determined using standardized methods with experimental instruments. Moreover, a pyrolysis analysis with computational methods will be performed based on the experimental parameters. Small-scale testing methods will be used to assess the flammability properties of five different polystyrene compounds. A graphene polystyrene masterbatch is qualitatively compared to expanded polystyrene samples with different compositions.

The second part of the thesis is focused to qualitatively evaluate the fire behavior of the polystyrene insulation using numerical simulations. Heat release rate values from Cone Calorimeter experiments with 10 mm thick polystyrene specimens will be used as input parameters for temperature evaluation on a large-scale model which resembles the BS 8414 testing procedure. The temperatures in front of the combustion chamber and the fire source will be validated against existing large-scale experiments performed in a testing set up following the standardized method.

## 1.2 Literature review

This section underlines the early pioneering activities intended to address the use and the assessment methods for the combustible materials that could be used as an insulation layer for the façade systems. It includes not only the first testing procedures developed by different countries around the globe, but also important findings which emphasize the different mechanisms related to the fire propagation over facades. As the core objective of this thesis is focused on the determination of the combustibility properties of different polystyrene compounds it is of interest to reveal important research findings in this field.

### 1.2.1 Research activities on facades in Sweden

Façade testing has a long history in Sweden. In 1958, Johanesson and Larsson [4] performed a series of large-scale experiments along with laboratory measurements aimed to determine the possibility of utilization and the methods of use for the combustible materials on the external walls of the existing buildings.

Another extensive study containing data from full-scale experiments was done by Ondrus who studied the fire behavior of the thermal insulation materials as part of a cladding system for the building facades [5]. Various thermal insulation systems for multi-storey buildings were exposed to the flames and hot gases produced by a single room fire. Hence, the insulation layer was directly exposed to the effect of flames and combustion effluents emerging through the compartment window. Not only the increased risk of flame spread over façade system and through the window of the compartment had been studied, but also the fire propagation within the compartment itself and the risk of spread due to falling parts from the collapsing façade.

During the initial series of experiments, they used apartment furnishings made of synthetic components which generated a rough fire load density of 110 MJ/$m^2$ of the total surface of enclosure. The testing facility was a three-storey construction made entirely from aerated concrete with the insulation layer placed on the front side to replicate the end use conditions. The total duration of each experiment was 10 minutes, which was intended to simulate a fully developed fire conditions inside a domestic apartment.

Three different cladding systems were investigated during these experiments:

- mineral wool insulation mounted on a wooden-studs frame and covered with steel and aluminum sheets;
- mineral wool insulation protected by a thick rendering layer of plaster;
- cellular plastic insulation protected by a thin rendering layer of plaster.

The final evaluation of the fire performance of the cladding materials was made by photograph footages, visual observations and measurement devices for temperatures inside the flames, external part of the walls and within the insulation, as well as for the heat flux imposed along the façade.

At the completion of the experimental work, the authors proposed a set of criteria for the classification and assessment of the façade systems, as follows:

- no observable collapse of large parts from the external insulation layer of the façade;
- the flame spread over the surface or within the insulation layer should be limited to the bottom part of the third floor window. The presence of the external flames which could ignite the eaves is not acceptable;
- there must be no fire spread to the second floor through the windows. This criterion was supposed to be fulfilled only when the heat flux imposed into the middle of the window

was not higher than 80 kW/$m^2$, which corresponded to the observed limit of failure for the glass panes.

The first two criteria were recommended for buildings up to four floors, while for those up to eight floors they can only be applied if there is a possibility for the external fire extinguishment. In addition, when the building height exceeds eight floors or there is no access for the outside fire extinguishment for those between five and eight floors, the third criterion from the requirements must be applied.

Nowadays, this testing method forms the basis of the so-called SP 105 [76]. According to the Swedish regulations all the façade insulating materials must be non-combustible or they should pass the large-scale test criteria provided by the above-mentioned document.

### 1.2.2 Research activities on facades in Japan

In the early 1960's, Yokoi had started to investigate different fire protection strategies to limit the vertical flame spread between openings in the facades [6]. As the architectural trend of that time shifted towards large windows design, the risk of fire spread between the window openings increased, mainly due to small spandrel dimensions on one hand and the lack of fire-resistant materials on the other. Thermal radiation and the convective effect of the hot rising gases may cause the window glass breakage and could ignite the combustible materials on the storey above. Therefore, the Japanese authorities decided to conduct both full-scale and small-scale experiments aimed to respond to these new emerging construction technologies.

The use of horizontal projections between floors to deflect the flames away from the façade of the building has been investigated [7]. Based on small-scale work, he found an interesting relation between the width of the horizontal projection and the trajectory of the rising plume. The experimental results suggested that a relatively small apron was able to limit the flame spread when the shape factor was sufficiently small, but it significantly increased when wider windows were used and the impingement of the flames was less. Moreover, it was discovered that there is a similar behavior when the flames are projected further away on a higher level by the horizontal apron with the situation when there is no horizontal extension on the outer part of the building.

The final research report led to recommendations related to the width of the horizontal projections as well as to mathematical methods to calculate the minimum dimensions of the necessary spandrel. It was emphasized that a horizontal projection gives better results in terms of fire spread when the width of the window is longer than its length. The explanation behind this theory is that the flames generated through this type of openings do not exhibit such a long vertically height, providing a better screening against the rising plume. A tabulated method to calculate the height of the spandrel when the rising plume reaches the temperature of $500^0$ C was proposed, while a minimum 0.74 m deep horizontal apron was

adopted by the Japanese Ministry of Construction for the revised building code version of that period.

Furthermore, Hokugo et al. [8] explored the fire propagation mechanism through multiple-storey building balconies. They discovered that the addition of the PMMA on the vertical side of the balcony combined with the combustible materials placed on the unexposed side of the fence augmented the total heat release through multiple burning materials in the same time.

### 1.2.3 Research activities on facades in Canada

Since 1967, McGuire had studied the vertical flame spread characteristics of the external cladding components. Several cladding solutions fixed on a concrete wall were exposed to a propane-fired burner which produced a 0.5 m high flame. The flame jet was directed towards the bottom edge of the specimen, in such a way that the baseline of the assembly was flushed by the flames. Hence, he noticed that the tested systems behaved in one of the two ways: either they propagated fire upwards within a short time after ignition, or they made little contribution to the flames [9].

Later at the end of 1980's decade, the National Research Council of Canada developed test methods intended to determine the flammability contribution of the combustible insulating materials. Through a long term experimental study, which included full-scale and reduced-scale facilities, they evaluated the fire hazards associated with the use of combustible façade assemblies and the influencing factors of the thermal exposure on the external walls.

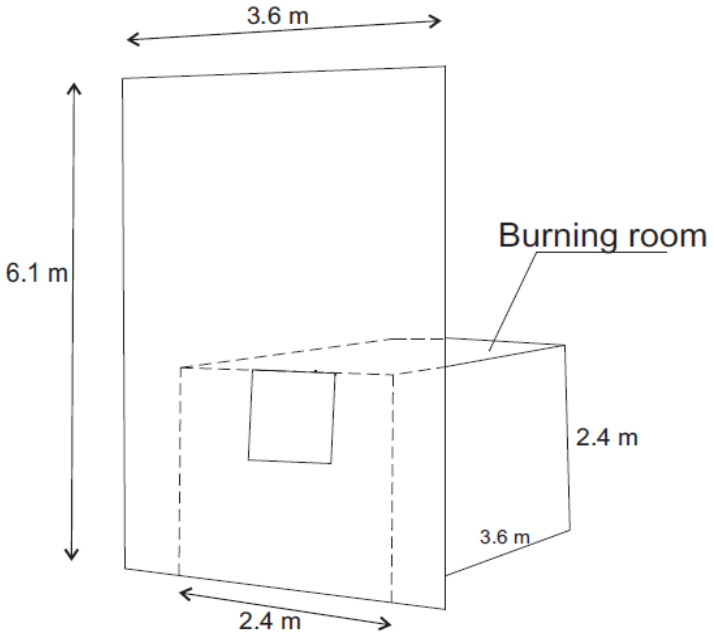


Figure 2 Smaller facility used for the Canadian tests (redrawn from [10])

Oleszkiewicz was appointed by the Canadian authorities to conduct the experimental studies. He performed a series of three experiments in two different testing rigs with a wooden crib fire, were the total heat transfer to the wall and the influence of the radiation and convection components to the wall above the window were investigated. The smaller testing facility used to study heat transfer to external wall was a 2.4 m wide by 3.6 m deep by 2.4 m high compartment with the front side extended to 6.1 m in height and 3.6 m in width as shown in figure 2.

The other three wood crib fires were performed using a larger testing facility. This consisted of a three storey high construction made of concrete frame with a ground floor burning room and a concrete front wall covered with a non-combustible board. Another trial experiment using propane gas burners were conducted in the same three-storey facility in order to evaluate the impact of heat release rate in conjunction with window dimensions, on the heat transfer process to the external wall. Two years later from the beginning of the experiments he published another paper which clearly demonstrates the importance of the horizontal projection during an external fire [11]. He concluded that the emerging flames through a window can pose a severe thermal attack to the façade and this exposure increase with the heat release rate development, since part of the combustion process takes place out of the compartment in the close region of the exposed cladding. The larger the window dimensions, the more air entrainment to sustain the combustion inside which leads to a decrease in the external plume temperature and height of the flame portion outside. Furthermore, it was found that the horizontal projection has an important influence on the heat flux density imposed over the external façade, as depicted from figure 3 [10].

Not only the horizontal apron had an improvement on the safety design of the façade, but also the vertical dimensions of the spandrels. At least 2.5 m spandrel was needed in order to get a 50 % reduction of the incoming heat flux over the façade.

The performance of different cladding systems was categorized into three groups according to the flame spread indicated during the experiments. The performances were determined as follows [12]:

- no flame spread – specimens which did not support the spread of flame beyond the extent of the external flame;
- limited flame spread – the recorded flame spread distance on the specimen stopped or receded before the end of the test;
- unlimited flame spread – the recorded flame spread extended to the top of the wall.

All the above requirements and the tests methods were included in the Canadian Standard CAN/ULC S134-13 – Standard Method of Fire Test of Exterior Wall Assemblies, intended to evaluate the fire performance of façade assemblies under controlled conditions representing the fire exposure resulting from a post-flashover fire in a compartment venting through an opening in the wall. Due to these intense research activities, the Canadian

regulations require that the heat flux at 3.5 m above the window to be less than 35 kW/m$^2$ and the flames do not spread more than 5 m in the vertical direction.

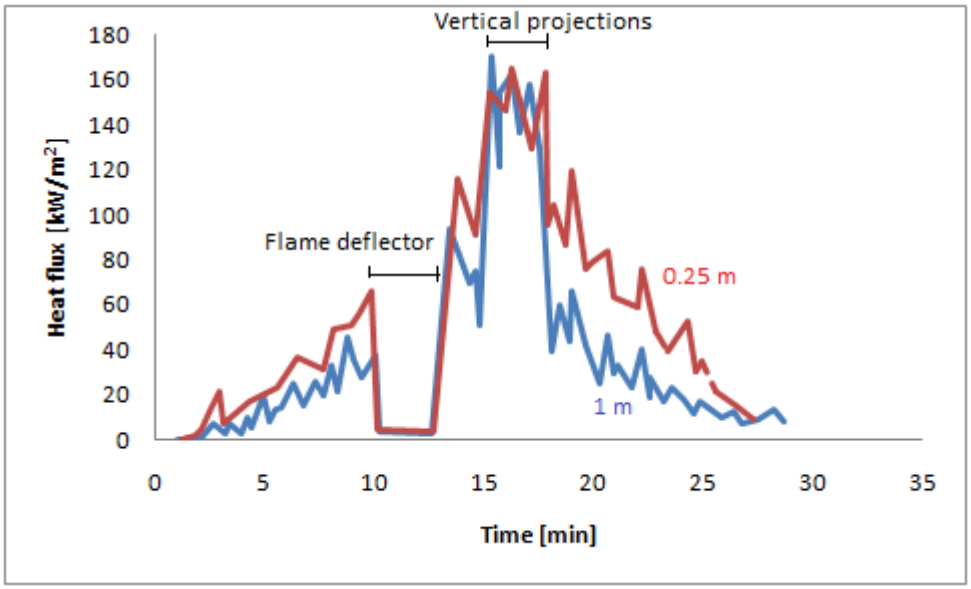


Figure 3 Variation of heat flux to the wall at different heights

above the window caused by the wall projection (redrawn from [10])

Nevertheless, more recent studies reported by Sumathipala [12] reveal that the effect of the re-entrant corner of the wall has a significantly influence on the fire hazard, especially when it is placed near to the margin of the window opening.

### 1.2.4 Research activities on facades in the United Kingdom

The BRE Fire Research Station and Scottish Laboratory developed a testing program aimed to investigate the fire performance of the external thermal insulation for the multi-storey building facades [13]. All the experiments were conducted on a four-storey facility, with a recessed opening where a 400 kg wood crib was placed giving a 3 MW heat output over a period of 25 minutes. The 9.2 m testing rig was erected inside the FRS Cardington Laboratory and it was provided with instrumentation devices to measure temperature and heat flux values on different points over the façade and the radiated heat likely to fall on the neighboring buildings.

The experimental wooden cribs were designed to sustain a fully-developed natural fire for at least 20 minutes with flames impinging on the façade to a minimum 2 m height over the recessed opening. During the experimental work eight insulating systems sandwiched between rendering and wall with other seven insulation materials protected by a ventilated cladding were tested on a heat flux of at least 100 kW/m$^2$. It was noted that the radiation produced by the burning cladding itself was not high enough to affect the adjoining edifices. Moreover, the wooden cladding was recommended only for low rise structures with a maximum height of 15 m to avoid vertical propagation of flames over the external surface.

The main conclusions of the BRE research program are summarized as follows:

- all the combustible insulating materials may be used without a specific design only if they shown satisfactory performance through a large-scale fire test;
- limited fire spread may be achieved for combustible materials embedded in non-sheeted systems only if:
  - cementitious rendered metal lathing over thermoplastics is provided with sufficient metal pins to avoid cladding collapse, while fire barriers needs to be installed every two floors from the second storey above;
  - cementitious rendered metal lathing over thermosetting products is provided with at least one metal pin per square meter to provide stable anchoring for the cladding system;
  - a small rendering with glass fabric reinforcement over thermoplastics in conjunction with fire barriers may be used provided that barriers are installed at every floor from the second storey above;
- all sprayed foamed insulating materials containing polyurethane or polyisocyanurate covered by a flame retardant layer are not suitable for multi-storey building facades;
- whenever combustible insulation products with sheeted over cladding systems are used, a fire barrier should be incorporated in the ventilated cavity every two storey in order to avoid the vertical flame spread.

Later on, the same research institute was involved in a joint program with insulating materials manufacturers to develop a large-scale testing method and an evaluation procedure for the performance of the cladding systems. This method was intended to evaluate the comportment of the non-loadbearing wall systems when exposed to fire. It included cladding assemblies, overcladding rainscreens, curtain walls and exterior finishing systems (EIFS) as reported by Morris [14].

All the efforts and the intense activities of Building Research Establishment had led to the development of the BR 135 which sets out the principles and design methodologies for fire performance of external thermal insulation for walls of multistory buildings. In its third edition revised by Colwell and Baker [15] outlines the performance of currently used materials and technologies, while offering various scenarios based on typical examples of nowadays practice.

## 1.3 Past incidents involving facade systems

Each of the following examples involving polystyrene insulation has been chosen to better describe various fire propagation mechanisms on façade.

### 1.3.1 Apartment building, Berlin – Germany, 2005

A deadly fire occurred on an apartment building in Treskowstraße Pankow, Berlin on the 21st of April 2005. The fire started on the second floor (figure 4) of this seven storey block of flats and spread rapidly on the façade to the entire height of the building leading to three injuries and two tragically fatalities.

Figure 4 Façade fire in Berlin, 2005 [16]

The insulating system was mounted on a 25 mm thick chipboard structure which was the remaining formwork for the existing concrete external walls. It consisted of eighty millimeters flame retarded expanded polystyrene which was encased with an external mesh and a thin rendering layer. Although a 500 mm mineral fibre fire barrier was added to the second and fourth floor in 2004, the resulting fire ignited the EIFS system and advanced up to the top of the building in less than 20 minutes. Witnesses reported that emerging flames through the windows of the room of origin spread into the levels above producing a significant smoke spread over the entire compartment. This is one of the examples where leapfrog effect is clearly evidenced.

### 1.3.2 MGM MONTE CARLO Hotel, Las Vegas, USA, 2008

A fire started in the 32-storey Monte Carlo Hotel and Casino on the 25$^{th}$ of January 2008. EIFS containing expanded polystyrene foam encased with lamina was installed as the exterior cladding of the building. This system was provided on the flat areas of the construction and on the decorative columns between 29$^{th}$ and 32$^{nd}$ floor.

An additional polyurethane resin with polystyrene foam was also installed to protect the architectural details of the edifice. These materials were included on the horizontal strip at the 29$^{th}$ floor and the top part of the 32$^{nd}$ floor as well as on the railing at the top of the parapet wall above the building. Due to some welding operations on the roof near the parapet wall, the exterior cladding materials were ignited on the left side of the central area. Following the ignition, the fire progressed laterally over decorative materials (figure 5) and combustible cladding and broke several windows, but the sprinkler installation efficiently suppressed any fire spread to the guest rooms.

Figure 5 MGM MONTECARLO façade fire, 2008 [17]

Clark County Nevada and Hughes Associates who performed the investigation pointed in their report that EIFS was protected with a non-compliant layer of lamina. Due to large burning droplets of expanded polystyrene and polyurethane, the fire extended to the decorative elements from the 29$^{th}$ floor. Over the time, the fire moved to the adjacent towers creating a lateral flame front, but it did not spread downwards to the rooms located beneath the 29$^{th}$ floor. Moreover, it was reported that the primary contributor to the progression of the fire was the combination of materials in the decorative band at the top of the wall, the decorative band at the top of the 32$^{nd}$ floor and the elements in the medallions. Although the fire progressed over these materials, it was concluded that the EIFS system was not the primary cause of the continued progression of the fire [17].

### 1.3.3 Apartment building, Miskolc - Hungary, 2009

An eleven storey residential building with a façade made of polystyrene based EIFS was exposed to an external fire on the 15$^{th}$ of August 2009, in Miskolc, Hungary. The fire started in a 6$^{th}$ floor apartment kitchen and spread on the combustible façade up to the top of the building, resulting in 3 fatalities. The fire also resulted in smoke spread through the stairwell and the elevator hoist [18].

The existing apartment building was refurbished in 2007, but according to the responsible authorities the materials used for thermal insulation were not a certified EIFS system. In the aftermath of the incident the fire investigators revealed that the inadequate fixing of lamina to the polystyrene slabs and the lack of fire propagation barriers contributed to the external fire spread as depicted from figure 6.

The inadequacy of the fastening systems could lead, in general, to the collapse of the façade parts, which in turn may form other fires at the base of the façade. Once the ignited parts reach the ground level the will rapidly ignite the bottom part of the facade that could have been saved from further flame propagation.

Figure 6 Façade fire in Miskolc, 2009 [19]

### 1.3.4 Immigrant hostel, Dijon – France, 2010

Seven people died and eleven were seriously injured by a fire in a nine storey immigrant hostel located in the eastern French city of Dijon. On the 14$^{th}$ of November 2010 a fire was reported to spread from a burning waste container over the façade.

The EIFS system with expanded polystyrene insulation generated a rapid vertical propagation of fire and significant smoke spread throughout the building. It was reported that more than 130 people were evacuated during the incident, while some of the inhabitants were jumping from windows to escape from the inferno. Three of the 93 firefighters who battled the blaze also suffered from smoke inhalation [20].

Neither the thin organic render applied on the façade, nor the mineral wool fire barriers were effective in preventing the flames from igniting the insulation and spreading upwards along the façade. From the figure 7 displayed below, it appears that much of the vertical flame spread is concentrated on the vertical channel profile created by the balconies [21].

Figure 7 Façade fire in Dijon, 2010 [21]

### 1.3.5 Apartment building, Târgu-Mureș – Romania, 2012

A 10-storey block of flats façade caught on fire on the 7th of July 2012, in Târgu-Mureș, Romania. The newly retrofitted cladding was part of the national thermal rehabilitation program which followed the European legislation requirements. According to the fire brigade investigators the fire started on a mercantile storage space placed on the ground level of the building in the proximity of the façade elements.

Figure 8 Façade fire in Târgu-Mureș, 2012 [22]

The EIFS system containing expanded polystyrene was lit on a short time following the ignition and rapidly propagated on the west side of the combustible façade. It was noted that the fire propagation to the upmost level of the flat took nearly 10 minutes, but no casualties were reported. In the investigation report was emphasized the lack of combustible barriers, while the non-complying fixing system of the EPS sheets led to falling burning parts of the insulating layer.

### 1.3.6 Karlstad Hospital, Karlstad – Sweden, 2013

A fire broke out at the Central Hospital in Karlstad on 29 August 2013. The incident took place on a new part of the hospital that was under construction [23]. The EIFS with polystyrene insulation has been chosen to decorate the external part of the building. The combustible façade insulating system allowed the fire to rapidly spread up the outside of the construction. Moreover, the flaming droplets and burning parts of polystyrene caused the development of new small fires over the scaffolding mounted in the proximity of the blazing façade, as shown in figure 9.

Four wards with more than 60 patients were evacuated as dense smoke and hot gases progressed inside the compartment. Only two injuries were reported among the construction staff as they were trying to extinguish the fire and inhaled toxic combustion products.

Figure 9 Façade fire in Karlstad, 2013 [24]

An important aspect in the development and flame spread mechanism during façade fires is represented by the burning droplets which can ignite not only the bottom façade itself, but also any other combustible materials from its vicinity.

# 2. TECHNICAL PERFORMANCE OF FAÇADE SYSTEMS

## 2.1 Types of façade systems

There is a wide variety of construction materials that can be used for the construction of the building facades. Even if it is a glazing façade or a cladding applied on an external wall, they all should limit a self-spreading fire up to the wall, either through the outer surface or through the concealed spaces within the wall. Typically, the international fire safety codes require that materials for the façade assembly to be non-combustible or at least limited combustible. In general, these requirements are applicable for high-rise buildings or skyscrapers, but there is still a wide range of buildings were combustible components are in use. It is to understand that a review of combustible façade systems is of interest for this thesis work, especially those containing a polystyrene insulating layer.

A broad range of different types of combustible exterior wall assemblies are in common use, including exterior insulated finish systems (EIFS), metal composite cladding, high pressure laminates, insulated sandwich panels, rainscreen barriers, external timber panels and a range of other systems. These exterior wall assemblies are complex structures of different components and layers which may include vertical cavities with or without fire stopping [19]. Due to this complexity, the fire performance assessment should be performed for the entire system with all the components in place as per end use conditions.

### 2.1.1 Exterior Insulating Finish Systems

EIFS is a general class of non-load bearing building cladding system that provides exterior walls with an insulated, water-resistant, finished surface in an integrated composite material system [25]. The product is also traded as synthetic stucco and it is similar to External Thermal Insulation Cladding System (ETICS) used across Europe. This external wall substrate has been seen as a rapid and cost-effective solution to enhance the thermal insulation properties, weather protection and external design. Rigid insulation boards on the external part of the wall sheathing are often used for its construction. It may be applied on a different construction material and is typically lined on a suitable substrate such as cement or gypsum boards. The entire system is usually fixed to the support structure with professional adhesive or mechanical procedures.

Two different types of EIFS can be distinguished: a polymer based system which has a reinforced base coat applied to the insulating layer prior to the finish cover application and the second less common type is the polymer modified system. The insulating material for the first one is the expanded polystyrene (EPS), while for the later the extruded polystyrene (XPS) is always used. For the modern applications a waterproof and drainage system are included to provide a weather shield and to extend the lifespan of the construction. Therefore, all the water-resistant EIFS ensembles rely primarily on the base coat portion of the exterior skin to resist water penetration [26]. In this case a membrane barrier is placed

over the substrate and small cavities are created between the water resistive barrier and the insulating layer when installed.

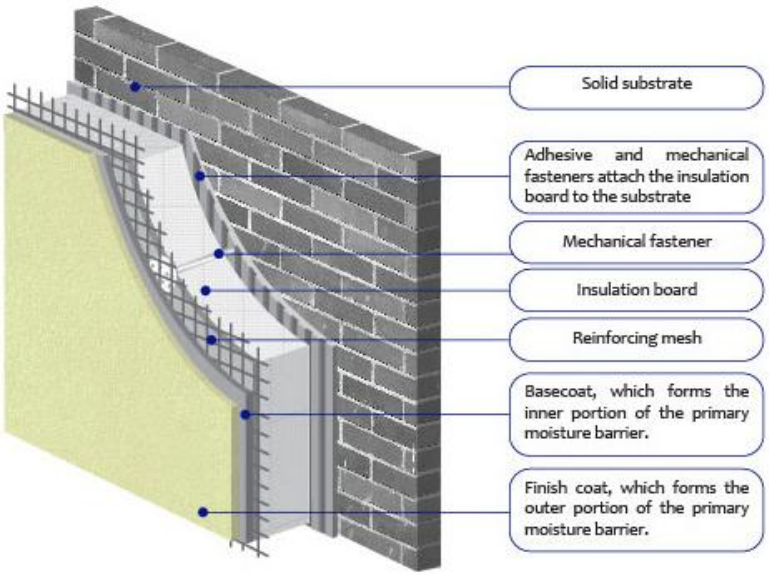


Figure 10 EIFS system with reinforced polymer based coating [27]

This multi-layered exterior finish is generally installed in the following order (figure 10):

- an optional water-barrier that is typically fluid applied and covers the solid substrate;
- adhesive and mechanical fasteners to attach the insulation sheets to the supporting structure;
- mechanical fasteners used to fix tightly the system to the building structure;
- insulation board fixed with adhesive or mechanical fasteners to the substrate;
- base coat which forms the inner portion of the primary moisture barrier. This is an acrylic or cement based polymer applied on the top of the insulation that it is often resistant to ignition;
- reinforcement mesh that is included in the base coat material;
- Finish coat, which forms the outer portion of the primary moisture barrier.

### 2.1.2 Metal composite cladding

Metal composite panels known also as metal composite materials (MCM) are generally used in the external façade of buildings. These wall panel systems are a successful combination of aesthetics and affordability which makes them very popular among designers. They are in a form of thin section panels with a core material sandwiched between two metal sheets as shown in figure 11. The insulation material is usually a mixed polyethylene with mineral filler or a low density polyethylene (LDPE) and typically ranges from 2 and 5 mm thickness. The metal component is available in a wide range of shapes and profiles and can be aluminum, steel, zinc or copper. Modern manufacturing techniques allow metals to be pre-aged, coated with preservatives, or painted in a wide range of nuance and texture [28]. Not only they can be mounted vertically, horizontally or skewed, but also to the curvilinear shaped facades.

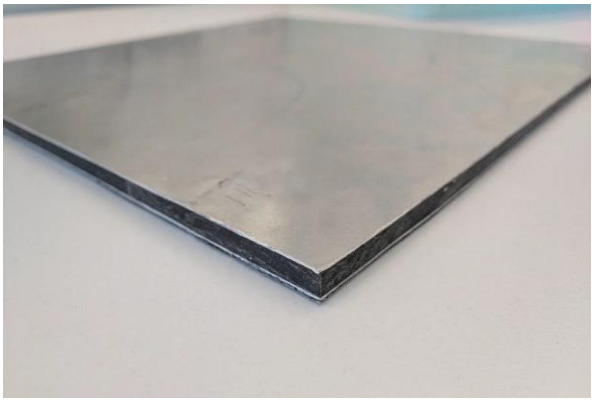

Figure 11 Sample piece of an Aluminum Composite Panel [29]

Metal composite panels are usually assembled on site, and generally consist of four components [30]:

- a thin internal material to ensure air tightness;
- insulating material such as polyethylene composite or mineral wool;
- spacer brackets to support the metal sheets;
- profiled metal facing sheet to provide weather protection.

In general, the composite panels are placed on steel channels or battens which will create a 40 mm air gap between the supporting structure and the cladding. They are fastened to the steel channels by one of the two following methods [30]:

- flat stick method – a double sided adhesive tape is used to stick the panels to the steel structure;
- cassette mount method – they are designed with interlocking systems for quick installation in which the edges of the panels are folded at right angles and screw tighten to the steel structure.

### 2.1.3 High pressure laminates

A laminate is a man made decorative material that is applied to the surface of a substrate. It is often referred to as HPL, or high pressure laminate, but its technical name is thermosetting high pressure decorative plastic laminate [31]. The most used manufacturing procedure involves high pressure and temperatures, giving a stable, dense panel and a good strength to weight ratio, while having a good weather protection properties. They are comprised of multiple layers of Kraft paper impregnated with resins. Three layers of paper are introduced into a press which applies at the same time heat and pressure to allow the thermoset resin to impregnate into the paper giving a consolidated sheet with a high density. The thermosetting resins will then undergo a curing process that creates, through a cross linking phenomenon, irreversible and strong chemical bonds inside the rigid laminate.

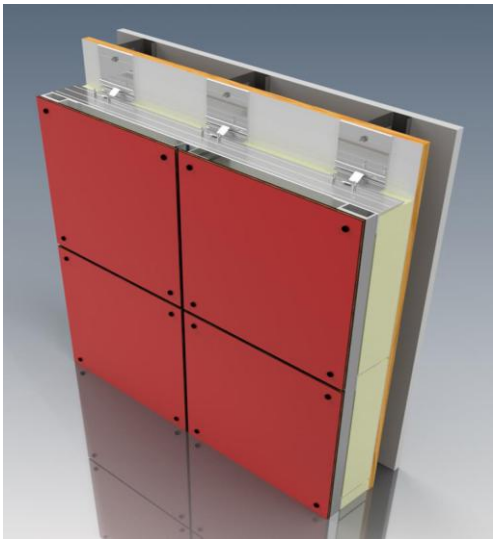

Figure 12 HPL mounting detail for facades [32]

The series of the European Standard EN 438 cover the requirements and specifications for high pressure laminate sheets based on thermosetting resins. They can be used for vertical exterior wall coverings such as façade cladding, balcony panels, sun louvers as well as horizontal exterior ceiling applications [33]. In the recent years they are preferred for use in newly ventilated facades design as a combination with other materials or a single layer applied on the external support substrate.

It is important to know that during the cutting process the overall dimensions of the panels might change due to moisture absorption. They are usually installed over the existing substructure using metal channels that will create a cavity between the panels and the supporting wall. Exposed screws and rivets are used to fix the panels to the metal channels as shown in figure 12. For thicker panels, clearly defined fixed and sliding brackets or special clips may be used to tighten the entire ensemble.

### 2.1.4 Structural insulation panel systems

A structural insulated panel is a form of sandwiched panel which contains an insulating foam core between two structural facings. These two layers of structural board can be metal sheets, plywood, gypsum plasterboard, cement, OSB or magnesium oxide boards. The internal insulating foam can be expanded polystyrene, extruded polystyrene, polyisocyanurate foam, polyurethane or composite honeycomb [34].

These engineered panels may be used for many different applications such wall, ceiling, floor and foundation systems. They can combine several components of the building to provide a strong, durable and energy efficient design feature. Structural insulation panel systems are a common solution for various commercial and residential applications and are compatible with other occupancies due to their fast construction and site adaptability. It is often used by architects as an alternative to standard construction materials.

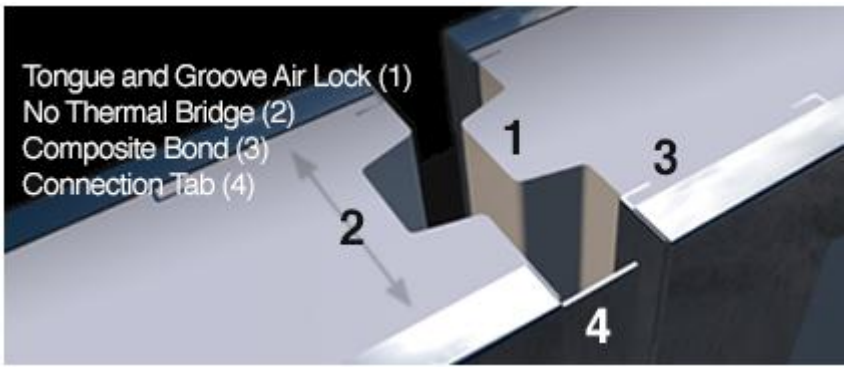


Figure 13 SIPS mounting detail [35]

Most of the panels are connected through an interlocking technique with a tongue and groove air lock joints and self-bond composite materials as depicted from figure 13. All the panels are placed on a bottom track along the perimeter of the site and screwed together at the leading edge. Furthermore, another connecting track is mounted on the top of the panels forming a strong and versatile assembly.

### 2.1.5 Rainscreen cladding

Rainscreen cladding is an innovative method used to provide weather protection for the building structure and the external wall elements. Rainscreen cladding consists of an outer decorative layer fixed to an underlying structure using a supporting mesh which provides a ventilated and drained cavity between the structure and façade components.

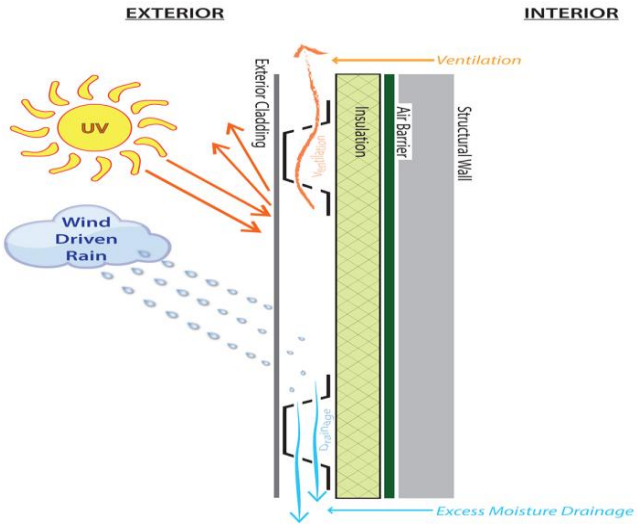


Figure 14 Rainscreen assembly [36]

A typical example of rainscreen shown in figure 14 includes the structural wall, the insulation layer, the ventilated cavity with supporting brackets and an exterior cladding panel. Generally the wall substrate is lined with an additional grade sheeting product containing cement, gypsum or timber board covered with a water-resistant membrane.

This type of external system is not normally sealed and a ventilation cavity of at least 25 mm is allowed immediately behind the cladding panel. Typically, the insulation panels consist of polyurethane, polyisocyanurate, expanded polystyrene or mineral fibre based materials. Although insulation sheet is placed within the cavity, the openings provided at both top and bottom edges of the clad will allow a continuous evaporation of the moisture without the risk of interstitial condensation or structural decay [37].

## 2.2 Fire propagation mechanism over facades

In general, there are different initiating scenarios for the façade fires. These fire sources can be divided in to the following main types [77]:

- an external fire to the building from a ground fuel package ignited near the wall or other burning building placed in the vicinity of the façade as shown in figure 16;
- an internal fire that will result either in window breaking and projecting flames over the façade or penetrating the fire-resistant partitions;

The upward flame spread mechanism consists of three primary regions as depicted from figure 15. The pyrolysis zone in the $x_p$ region where the burning material produces the combustible volatiles contributing to the flame rising. In the second region extending between $x_p$ and $x_f$, known as the combusting flame, the excess volatiles continue to burn and preheat the unburnt solid fuel, while above the height $x_f$, in the buoyant plume, the combustion products are formed and mixed with the entrained air from the surroundings.

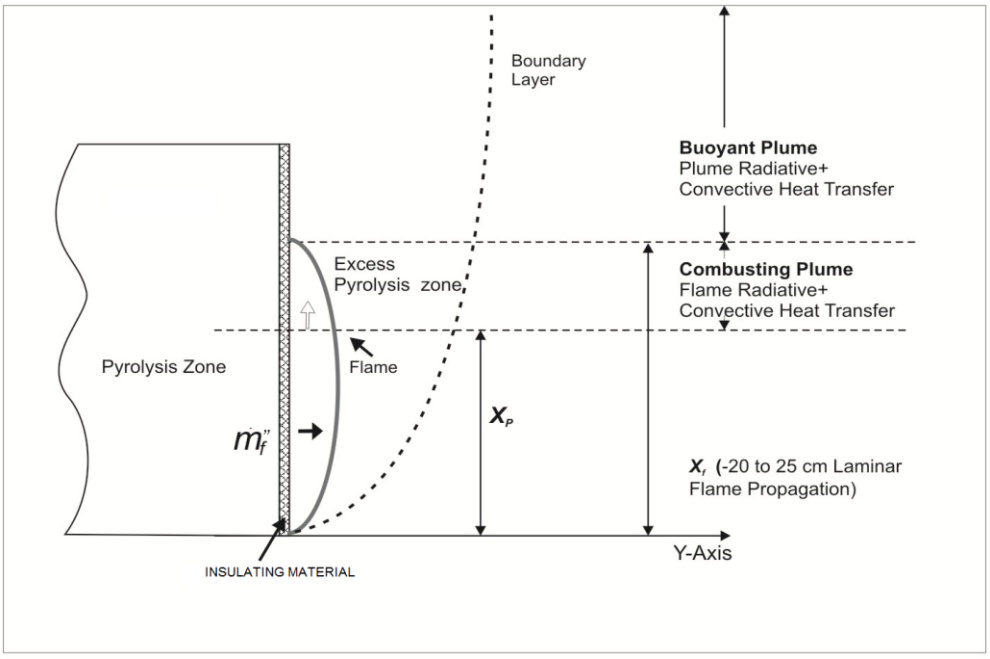


Figure 15 Theoretical vertical flame spread mechanism (adapted from [38])

The propagation process is influenced by the heat flux imposed from the flames to the surface of the material ahead the pyrolysis front. When flames are small and laminar the rate of spread follows $x_p \sim t^2$ for thermally thick materials, whereas for turbulent and large flames it increases exponentially with time. Several models have been developed to analyze the upward flame spread. As the rate of lateral and downward flame spread is always orders of magnitude lower than vertical spread, these processes are neglected in the analysis [39]. The vertical flame spread analysis is a complex process which involves different parameters that are difficult to be coupled and yet research activities need to be performed in order to develop a reliable model.

The key mechanisms which contribute to vertical fire spread include:

- leapfrog effect which is encountered in mid-rise and high-rise building fires where flames are merging out through the window perimeter resulting in level to level fire spread, see figure 16, (3);
- flame spread over the external surface of the combustible cladding materials;
- chimney effect appears in the cavity between the edge of the floor slab and the exterior wall, where heated surfaces create thermal zones that include upward air movement, which in turn sucks hot gases and flames in its direction;
- heat flux impact causing loss of integrity of the noncombustible external layer resulting on flame spread on the internal insulating material [17];
- poke through effect which is generated by flames and hot gases that penetrate through openings to ignite combustible products on the other side of fire resistant partitions;
- flaming droplets and burning parts creating secondary external fires to lower levels;
- trench effect can be generated by channeling of convective heat and radiation between corners leading to concurrent spread at higher inclinations.

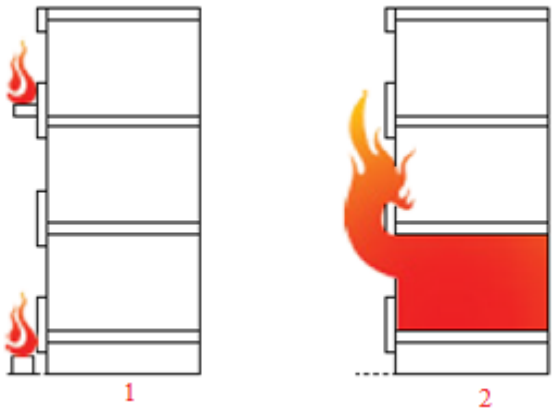


Figure 16 Typical scenarios of vertical fire spread (redrawn from [40])

The main factors involved in the fire development in façade systems are listed below [41]:

- readily façade material combustible core (insulation, sealants, joints, panels);
- inferior façade panel integrity;

- non tested façade, sealant and fire stopping systems;
- poor installation of façade and fire stopping systems;
- lack of thermal and cavity barriers;
- in field panels not as tested;
- ageing of a façade system.

## 2.3 Performance criteria established by international standards

There are various international testing standards used for the assessment of the façade assemblies, but not all of them are embedded in the building code requirements. The approval process may or may not ask for a specific test and it is different from one country to another. According to the European Commission study [42] related to the development of a new assessment method for fire performance of facades, all the responding countries to the questionnaire indicated that they have regulations and guidance governing the fire performance of facades. These regulations are covered in general by the European reaction to fire and fire resistance system.

Construction Products Regulation no. 305/2011 lays down harmonized conditions for the marketing of construction products within the European Union market. This regulation establishes a series of requirements for the construction products in the internal market to eliminate the technical barriers in this field. These requirements are stated in a form of harmonized technical specifications for the purpose of assessing the performance of products and to ensure the essential characteristics of a construction material. The European Organization for Technical Assessment (EOTA) published the ETAG-004, which is a guide related to the External Thermal Insulation Composite Systems with Rendering (ETICS) that specifies the minimum performance criteria and the assessment procedure used to evaluate the intended use and the presumed conditions for the design and execution of these systems.

### 2.3.1 Temperature rise

The rise of temperature is one of the criteria set by many standards. There is a certain maximum threshold, which may differ from method to method. This maximum temperature is coupled with time ranges so that the specimen should not exceed the allowed value for a specified period. In other documents the temperature rise is linked with additional performance criteria, like flame spread, to determine the overall performance of the product.

According to BR 135 a maximum air temperature of $600^0$ C should not be exceeded at 50 mm in the front of the specimen and 5 m above the combustion chamber. Moreover, the temperature rise in the middle core of the insulating layer or any cavity at 5 m beyond the combustion place should not exceed $600^0$ C. The system is deemed to fail if this temperature has been exceeded for a period of at least 30 s, within 15 minutes of the testing start time. The maximum temperature rise imposed by the Swedish method - SP

105, is $500^0$ C for more than 2 minutes or $450^0$ C for more than 10 minutes measured at the top part of the specimen. DIN 4102-20 requires that temperature should not be more than $500^0$ C at 3.5 m above the window soffit or over the façade surface as well as inside the cavities or any internal gaps.

### 2.3.2 Flame spread

Both horizontal and vertical flame spread is evaluated for the insulating combustible core or the external surface of façade systems. Like the temperature rise criteria, the assessment method for the spread of flames may vary to a particular degree, depending on the experimental method. The most common and used criteria refers to the extent of the flame spread which may include no flaming at the top part or the lateral boundaries of the tested specimen. This performance criterion is often estimated by visual observations of the burning assembly or from examinations at the end of the testing procedure.

The British Standard BS 8414 uses the temperature rise recorded by thermocouples beyond a specified height, to evaluate both the internal and external flame spread. According to SP 105, there should be no flame or any damage caused by fire higher than the bottom soffit of the second storey opening, observed both on internal layers or external surface. A facade system is deemed to have failed as per DIN 4102-20 if continuous flames are observed at 3.5 m above the window soffit for more than 30 seconds.

### 2.3.3 Flaming droplets and burning parts

Wall cladding assemblies and external fixing systems should maintain their integrity and prevent their parts from falling for a minimum specified period of time. This is often an indirect performance specification and it is not detailed by the majority of testing procedures. There are some requirements related to the size and quantity of the flaming droplets or falling parts which could influence the final evaluation of the system.

Although the information related to this criterion will be mentioned in the testing report, the British Standard BS 8414 does not specify any requirements for it. According to SP 105 no large pieces are allowed to fall from the specimen. In the German method covered by DIN 4102-20 it is required that the duration of the falling of burning droplets and burning or non-ignited debris must not exceed 90 seconds after the burners have been turned off [43].

# 3. MATERIALS AND EXPERIMENTAL METHODOLOGY

## 3.1 Expanded polystyrene

Polystyrene is one of the first synthetic polymers manufactured at industrial scale. It has been seen as an alternative to the traditional materials and it is widely used in construction, packaging and other industries for its low cost, good thermal insulation and mechanical properties [44]. Expanded polystyrene is a petroleum-based foam obtained from styrene monomer by pressing the polystyrene pellets into molding machines and expanded under elevated temperatures from hot water or steam. The polymerization reaction takes place in a stirring reactor where the monomer and water mixture is heated up to $90^0$-$120^0$ C. At the end of the polymerization process, the mixture is cooled down until it will reach $50^0$, and the polystyrene pearls are separated in the centrifugal separator to remove all the remaining suspension agents.

Expanded polystyrene gets its excellent thermal insulating properties from the motionless air trapped within its cellular structure. As the total amount of air is nearly 98 % from the entire structure, the thermal conductivity values are relatively low compared with other available materials. These properties are strongly influenced by the temperatures and bulk density of the material. Increasing the density of the insulating boards will result in a thermal conductivity decrease which in turn gives better insulating characteristics. EPS has a partly open pore structure and the typical thermal conductivity ranges between 30 – 40 W/mK. One of the advantages of this insulating material is that it can be perforated, and also cut and adjusted at the building site, without any loss of thermal resistance [45].

Two different types of expanded polystyrene were used during the experimental measurements. The samples are produced by the same manufacturer and marketed under commercial nomenclature according to their declared densities (High density EPS and Low density EPS).

## 3.2 Graphite polystyrene

Graphite is one of the most stable forms of carbon, which proved to be safe and chemically inert. It occurs naturally with atoms arranged in a hexagonal structure and due to its high conductivity it is preferred in many electronic products such as electrodes, batteries and solar panels [46]. Graphite has very good infrared radiation absorbing capacity and a beam scattering behavior, too. The addition of graphite flakes in the expanded polystyrene structure will yield lower thermal conductivity than pure EPS. The inclusion of graphite nanotubes or carbon particles in the original EPS matrix will absorb the infrared radiation, reducing the thermal conductivity of the boards and their permeability to heat. Compared to most rigid insulators which perform by reducing convection and conduction components of heat loss, the infrared absorbers address energy loss through the radiation component, hence the R-value is increased.

While conventional EPS is white in color, the addition of graphite will turn its nuance to grey. This material may be used for a wide range of applications, such as external thermal insulation systems, cavity walls, roofs, bead injection or floors, both in new building work or in refurbishments. The thermal insulation performance remains unaltered over time and depending on its mass density, the thermal conductivity can vary between 0,03 – 0,032 W/mK [47].

The effect of expandable graphite on the flammability of polystyrene foams has been extensively investigated. It showed an improvement of the fire behavior, especially in combination with chemical flame retardants. Hosseinpour et al. found that the presence of the lignosulfunate as a surfactant improves the strength of fire retardant. However, the fire retardant test showed complete non-combustibility for foams containing 10 % of expandable graphite particles [48].

The characteristic fire parameters in this study were evaluated for grey graphite polystyrene with 3 – 7 % by weight graphite (Graphite EPS) and another mixed expanded polystyrene with both graphite and white pearls in an approximately even distribution (Mixed EPS).

## 3.3 Graphene polystyrene

Graphene is a single atomic layer of graphite in a mineral form which is an allotrope of carbon that contains very tightly bonded atoms organized into a single lattice. It is a semimetal with small overlap between the valence and the conduction bands that presents a zero-band gap characteristic. Graphene has emerged as one of the most promising nanomaterials due to its unique combination of properties. It has a strong electrical conductivity and thermal properties, being optically transparent, and yet so dense that is impermeable to gases, as not even helium can pass through its compact structure [49].

Graphene, a two-dimensional carbon material with excellent barrier properties, has been already introduced into polymeric materials to enhance their fire behavior. As a physical carbon source, graphene can reduce the heat release and inhibit the transfer of combustible volatiles during combustion [50]. Various research activities were aimed to develop a graphene polystyrene compound with improved electrical conductivity. The challenging part of graphene polystyrene preparation is represented by graphene dispersion throughout the polymer matrix by weakening the strong attractive forces between graphene sheets. One way to deal with this problem would be to obtain graphene oxide (GO) using Hummers' method, which can be better dispersed in polymers. Zhaokang Tu et al. [51] developed a facile, environmental-friendly method for graphene polystyrene preparation that involves the production of polystyrene latex microspheres with positive charges by introducing a cationic surfactant in the emulsion polymerization. Further, an in situ demulsification can be achieved through electrostatic adsorption of GO sheets with negative charges onto the positively charged polystyrene microspheres.

All the parameters used for the evaluation of the graphene polystyrene fire properties were depicted from research experiments conducted on a PS graphite masterbatch with 97 % polystyrene and 3 % graphene.

## 3.4 Measurement of flammability properties

### 3.4.1 Bomb Calorimeter

A bomb calorimeter is a self-contained apparatus used in the experimental determination of calorific potential of different samples in a pure high-pressure oxygen environment. A known amount of material is placed in a crucible and burnt in a sealed chamber. The assembled chamber containing the sample is immersed in a specified quantity of water with known heat of combustion determined from previous tests with a standardized combustible material. The water container is surrounded by an adiabatic protective shield which serves as a thermal insulator. An ignition fuse wire attached to electrodes is used to start the combustion inside the chamber, as shown in figure 17.

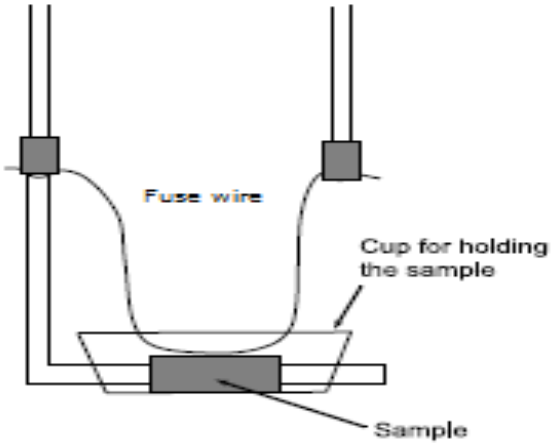


Figure 17 Bomb Calorimeter burning chamber [51]

Once the combustible sample has been ignited, the energy released is absorbed within the calorimeter. Knowing the resulting temperature change within the water container enables one to calculate the heat of combustion. If the specific heat in the surrounding environment is known, then the amount of heat released by material is given by:

$$H = \frac{\left( c_{pWater} \cdot \Delta T - Q_{E1} - Q_{E2} \right)}{m} \text{ [kJ/kg]} \qquad (3.1)$$

,where $c_{pWater}$ is the known specific heat for calorimeter system in kJ/kgC, ΔT is the temperature rise in degree Celsius, $Q_{E1}$ represents the correction value for the heat energy generated by the cotton thread, $Q_{E2}$ is the correction value for the energy generated from other burning aids and m is the mass of sample. Moreover, benzoic acid of high purity is involved in the calibration procedure of this testing apparatus.

### 3.4.2 Transient Plane Source (TPS)

The standardized TPS method is widely used for a simultaneously measurement of different thermal properties like thermal conductivity, thermal diffusivity and heat capacity. The basic principle involves a planar heat sensor in the form of a series of concentric circular line sources which is placed inside an infinite medium. This sensor will generate a constant heat into the sample which is influenced by the mean temperature of the source over time [52]. This thin metal spiral is made of electrically conducting nickel mounted between two insulating Kapton layers. Measurements could be performed on solid materials where the heating sensor is clamped between to flat surfaces of the tested material as shown in figure 18.

Figure 18 Typical set-up for TPS measurement

When electrical current flows through the spiral, heat is developed inside the metal that cause a temperature raise and thus the resistance of the spiral is changing. The rate of rise of this temperature is strongly influenced by how quickly the heat is conducted into the surrounding material. The heating process continues for a constant period of time, while the voltage across the sensor is continuously registered. The changes in the internal resistance of the spiral is direct proportional to the transient gradient developed on the surface of the sample and the electrical power applied to the sensor.

### 3.4.3 Microscale Combustion Calorimeter (MCC)

MCC is a small-scale testing apparatus which involves microscale samples to evaluate the flammability properties of combustible products. It utilizes pyrolysis-combustion flow calorimetry (PCFC), which principally combines the analytical pyrolysis, combustion gas analysis by oxygen consumption, and calorimetry flow. The two main principles of flaming combustion are separated in individually controlled reactors, into the solid-phase pyrolysis of the specimen and gas-phase combustion of the pyrolyzis gases [53]. In theory, the flaming combustion of solid phase is less efficient than premixed burning since the fuel and air mix solely for diffusion, so that the dimensional properties of the combustion region may be insufficient for a complete burning due to chemical kinetic or oxygen limitations. Therefore,

flaming combustion of solid phase could be a potentially inefficient process, while the non-flaming combustion in MCC is highly controlled and effective under specified conditions [54].

The most common methods for the determination of the specific kinetic parameters for thermal decomposition of the solid phase involve the thermo-gravimetric analysis, but the advantage of the MCC approach is that it allows a broad range of heating rates up to 5 K/s. The objective in the present report is to give a reliable estimation on the kinetic parameters, including activation energy and the characteristic pre-exponential factor. Thus, the evaluation will follow the methodology presented by Snegirev et al. [55], which consists of three main steps:

- evaluation of the apparent activation energy using the iso-conversional technique;
- expression of the conversion function by fitting the measured dependence of reaction rate on kinetic function;
- evaluation of the pre-exponential factor using the peak conversion function value and activation energy.

### 3.4.4 Cone Calorimeter

This fire testing apparatus was first developed in the early 1980s in the United States by Vytenis Babrauskas and it is based on the principle of oxygen consumption during the combustion process of materials. It is recognized to be the most important bench scale testing instrument to assess the flammability properties of various specimens. The oxygen consumption method was first identified in 1917 by Thornton who showed that for a large number of organic liquids and gases, a more or less constant net amount of heat is released per unit mass of oxygen consumed for complete combustion [56]. Based on these observations in the late 1950s similar measurements were started, but the original Cone Calorimeter was built by the actual National Institute of Standards and Technology.

The modern cone calorimeter consists of a numerous measurement devices and components aimed to measure different material parameters, as shown in figure 19. A cone-shaped electrical heater encased on a double-wall stainless steel cone is the main part of the instrument as it delivers the required incident heat flux on the surface of the material. Tested materials are placed on a square stainless steel specimen holder inside the load cell which weighs the sample during the experiment. Depending on the type and the characteristics of the assessed material, the sample holder can have either open or closed edges. A spark igniter device is placed below the heater at the surface of the tested material to ignite the flammable gases that are produced by the heated specimen. When the technician observes that the entire surface of the sample is burning, the ignition device is turned off and removed from the burning place. Hot gases and the combustion products from the sample are collected by an exhaust hood placed above the conical heater. All the

gases are forced by a gas ventilator to go out through a network of ducts where the rate of combustion products is measured.

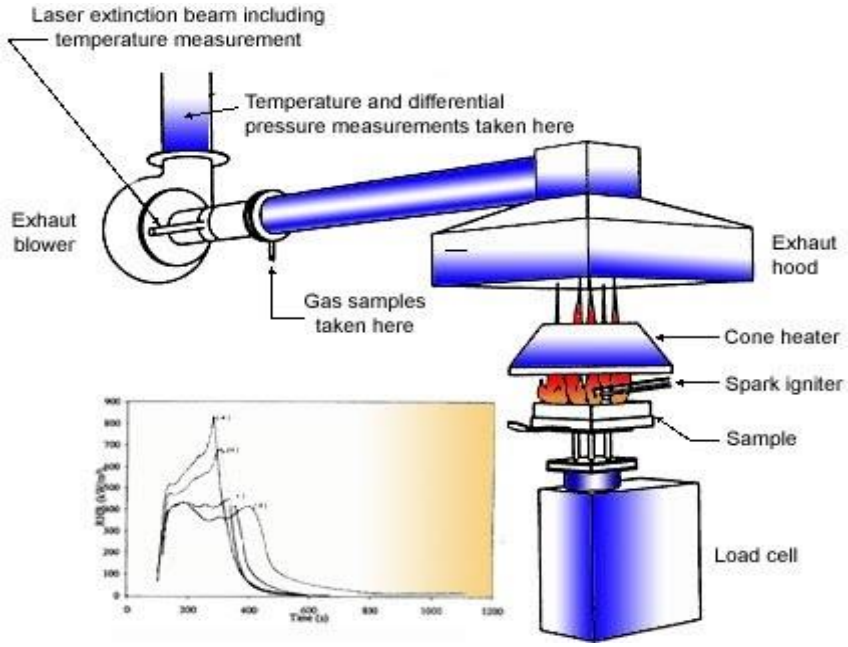


Figure 19 Cone Calorimeter set-up [57]

Before passing the gas analysers, the burning products are filtered to remove the particles and then a cold trap is used to eliminate the possible water from the smoke. Between the gas sampling place and the exhaust ventilator, a laser extinction beam including temperature measurements is placed. The standard orientation of the samples is horizontal, but vertical testing is also possible.

The main measuring functions of the cone calorimeter are:

- heat release rate;
- effective heat of combustion;
- mass loss rate;
- ignitability;
- smoke and soot;
- toxic gases.

Based on the ISO 5660-1 standard procedure the value of heat release rate has been calculated using the following formula:

$$\dot{Q} = 1.10 \cdot E_{O_2} \cdot x^0{}_{O_2} \cdot \left[ \frac{\Phi}{(1-\Phi) + 1.105 \cdot \Phi} \right] \cdot \dot{m}_e \qquad (3.2)$$

, where $E_{O_2}$ is the heat of combustion per unit mass of oxygen consumed, $x^0{}_{O_2}$ is the initial value of oxygen analyzer reading, $\Phi$ represents the oxygen depletion factor and $\dot{m}_e$ represents the mass flow rate of gases in the exhaust duct.

The oxygen consumption factor can be determined using the next expression:

$$\Phi = \frac{x^0{}_{O_2}\left(1 - x_{CO_2}\right) - x_{O_2}\left(1 - x^0{}_{CO_2}\right)}{x^0{}_{O_2}\left(1 - x_{CO_2} - x_{O_2}\right)} \tag{3.3}$$

The mass flow rate could be calculated from the pressure drop across the duct section and the temperature values at an orifice plate according to the following relation:

$$\dot{m}_e = C\sqrt{\frac{\Delta p}{T_e}} \tag{3.4}$$

, where C is the orifice flow meter calibration constant ($m^{1/2}g^{1/2}K^{1/2}$), $\Delta p$ is the orifice pressure differential (Pa) and $T_e$ is the absolute temperature of gas at the orifice meter (K).

### 3.4.5 TGA apparatus

This apparatus follows the thermogravimetry principle in which the mass loss of a sample is monitored against time. It measures changes in weight and the rate of change in mass as a function of temperature, time and ambient conditions. Measurements are used primarily to evaluate the composition of various materials and products and to predict their thermal behaviour and stability. This instrument can characterize components that exhibit mass loss due to chemical decomposition, reduction, oxidation or sorption of volatiles.

It consists of a sample pan that is held by an electronic balance. This pan is encased in a combustion chamber where it is heated or cooled during experiments. The gas content inside the furnace is precisely controlled by a sample gas purge. This atmosphere may be filled either with a reactive gas or an inert gaseous component that flows over the sample and exits through an exhaust network.

The TG technique is very popular in polymer research, in particular to study the thermal stability of polymeric systems under application conditions [58]. This is an ideal instrument to investigate thermal characteristics of nanocomposites. As during this study a graphene PS masterbatch that has unknown properties is used, this method is the most suitable approach to determine the reaction parameters.

Simultaneous Thermal Analysis (STA) was used for the assessment of the thermal properties of all the materials involved in this study. This technique combines the Thermogravimetry and Differential Scanning Calorimetry to measure both heat flow and weight changes in a microscale sample as a function of temperature in a tightly controlled environment. Simultaneous measurement of these two material properties not only improves the testing time span, but also simplifies the evaluation of the final results. The enthalpy changes can be precisely correlated to the TGA chemical steps resulting from the mass loss curve. Hence, the sequence in a thermal process could be easily identified in order to calculate the heat of reaction that determines the enthalpy difference between the products and the reactant.

## 3.5 Large-scale façade set-up description

The British Standard BS 8414 is a series of standards which sets out the requirements and performance criteria of non-loadbearing external cladding systems applied to the masonry surface of a building when they are exposed to an external fire under controlled conditions. This exposure is intended to be a close representation of both an external fire source and a fully developed internal fire that is being projected through an open window or by other means, leading to the cladding being exposed to the effects of external flames. Being an international used standard with clear criteria for temperature rise in the vicinity of the façade assembly, this method provides a comprehensive set of parameters for the numerical simulation.

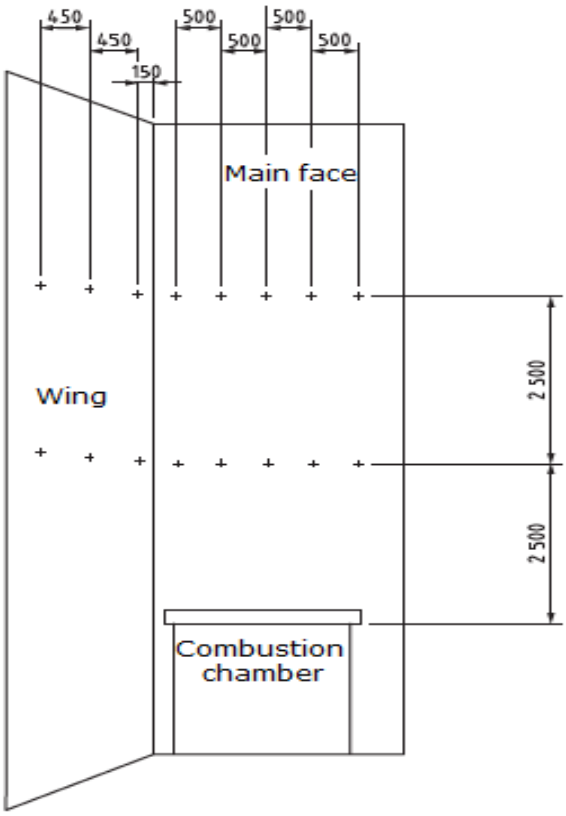


Figure 20 BS 8414 testing facility details [59]

The testing rig consists of a combustion chamber, an external L-shaped wall, an opening and measurement devices. Façade specimen should be placed on a structural steel frame which shall be designed and constructed to withstand the expected loading imposed by the system under test and any subsequent distortions that can occur during test program. It is a full-scale test in which a two-sided wall is constructed at right angles. Each wing is designed so that the minimum height above the combustion chamber is at least 2 m. The narrow side of the wall is 1500 mm, while the wide one is 2.8 m as shown in figure 20. The perpendicular line from the finished face of the cladding system on the re-entrant wing to the combustion chamber will allow a minimum distance of 260 ± 100 mm.

A wooden crib with a nominal heat output of 4500 MJ is placed inside the combustion chamber. It is designed to burn for approximately 30 minutes at a peak heat release rate of 3 ± 0.5 MW. This crib should be made of softwood sticks with square section side and a density that may range between 0.4 to 0.65 kg/dm$^3$. This fire source has to be placed on a solid platform positioned 400 mm above the floor of the combustion chamber. Dimensions of the combustion chamber opening are 2000 by 2000 mm so that the flames are projected towards the specimen [60]. The expected heat flux values could vary between 45 and 95 kW/m$^2$ at 1 m above the opening. This should be recorded for a continuous period of 20 minutes, but a typical mean value of 75 kW/m$^2$ should be expected.

Measurement devices should be placed on both faces of the specimen. Type K thermocouples with 1.5 mm bead diameter are mounted on two different levels at a specified spacing along the breadth of the walls. There are either external thermocouples positioned at 50 mm in front of the façade system, or internal ones that are inserted in the mid-depth of each layer within the insulating material. Additional heat flux gauges to measure the heat flux on the cladding system are placed on the same plane with the façade wall.

# 4. EXPERIMENTAL RESULTS

## 4.1 Bomb Calorimeter measurements

The Gross Calorific values of polystyrene samples were measured using a Bomb Calorimeter type IKA C200. The reference measurement procedure described in ISO 1716:2018 [61] and ISO 1928:2009 [62] was used in this work. Prior to the experimental measurement a calibration using benzoic acid with known properties was performed. All the trials were conducted using metallic crucibles with materials that had a mass varying between 100 and 250 mg, corresponding to their specific density.

The decomposition vessel was filled with pure oxygen in a proportion of 99.95 % at 30 bar to optimize the combustion process. Tests were repeated three times and the average value is presented in table 1.

Table 1 Heat of combustion results

| **Material** | **Gross heat of combustion [kJ/kg]** | | | **Mean value** | **Standard deviation** |
|---|---|---|---|---|---|
| Low density EPS | 39882 | 40564 | 41200 | 40548 | 659.13 |
| High density EPS | 40943 | 42168 | 42468 | 41859 | 807.9 |
| Mixed EPS | 40151 | 40190 | 40278 | 40206 | 65.05 |
| Graphite EPS | 34987 | 36295 | 37183 | 36155 | 1104.6 |
| Graphene EPS | 41174 | 41169 | 41268 | 41203 | 55,7 |

The addition of graphite in the polystyrene matrix improves the calorific potential of compounds with little less than 14 % compared with high density EPS. Even if the mixed EPS contains white polystyrene pearls, similar to those in the low-density component, the addition of graphite particles seems to be not so important in terms of heat of combustion results. Graphene polystyrene yielded a gross heat of combustion value among the highest from all the investigated specimens. This could be explained by the fact that this Graphene masterbatch is a molded and extruded product which presents a non homogeneous structure with a non uniform distribution of the graphene particles throughout its entire structure.

## 4.2 TPS measurements

Determination of thermal conductivity and heat capacity for solid samples was realized with a TPS 2500 S instrument according to ISO 22007-2 method [63]. Each specimen was tested for a period of 80 seconds on a 50 mW heat power. The approach used for this experiment, as described in the technical guide, is the isotropic powerful module in which the thermal

conductivity and specific heat represents the geometrical average value in the probed sample volume. The sensor used for this measurement has a radius of 14.6 mm and a thickness of 46 µm. This technique has the advantage that even a component of unknown properties can be easily tested and analyzed.

It is already known that both thermal conductivity and specific heat are changing with temperature increasing, but since the experimental method allows only an average calculation, the results presented in the table 2 are a representation of this approach.

Table 2 TPS results for thermal conductivity and specific heat

| **Material** | **Thermal conductivity [W/mK]** | **Specific heat [J/kgK]** |
|---|---|---|
| Low density EPS | 0.03036 | 1122 |
| High density EPS | 0.03102 | 1732 |
| Mixed EPS | 0.02922 | 1107 |
| Graphite EPS | 0.02763 | 1101 |
| Graphene PS | 0.1886 | 776 |

## 4.3 MCC measurements

A TC 12/53 Microscale Combustion Calorimeter was involved in this study to evaluate the flammability characteristics of various thermoplastic compounds. MCC is a relatively new testing apparatus in the fire safety engineering field, but compared to bench-scale methods it requires small amounts of material and it is very useful in the determination of kinetic particularities in the probed specimen. The measurement procedure for the assessment of heat release rate and kinetic parameters followed ASTM D 7309-11:2013 methodology [64].

Sometimes reliable heat release rate results are difficult to achieve as they are influenced by heating rate, the thickness of the specimen and the availability of oxygen in the burning environment. The MCC apparatus eliminates these uncertainties by using excess oxygen ambient and a controlled heating rate. Three different tests for each polystyrene compound were performed to determine the repeatability of the specific heat release rate (W/g) evaluation. All the samples were pyrolysed in pure nitrogen atmosphere with a combustor temperature fixed at $900^0$ C. Heating rate for these first trials was set at $60^0$ C/min for each triplet measurement. The order was randomized to help eliminate bias and systematic errors [53].

A set of parameters were chosen to emphasize the consistency and the repeatability of the results. The quantitative analysis of the MCC measurements is presented in the table 3 for peak heat release rate Q (W/g), temperature where the heat release rate reaches its peak T

($^0$C) and the specific heat release ΔH (kJ/g), which was calculated from integration of the HRR curve. A standard deviation of the results is also presented in the table below.

Table 3 MCC results

| Material | Q (W/g) | T ($^0$C) | ΔH (kJ/g) |
|---|---|---|---|
| **Low density EPS** | 765.954 | 444.47 | 37.901 |
| | 739.723 | 443.46 | 33.271 |
| | 742.558 | 444.015 | 34.363 |
| Mean | **749.411** | **443.981** | **35.17** |
| Standard deviation | 14.39 | 0.5 | 2.42 |
| Coefficient of Variation (%) | 1.5 | 0.09 | 5.6 |
| **High density EPS** | 790.594 | 443.216 | 37.586 |
| | 852.146 | 445.710 | 39.943 |
| | 847.219 | 442.27 | 38.910 |
| Mean | **829.986** | **443.732** | **38.813** |
| Standard deviation | 34.2 | 1.77 | 1.81 |
| Coefficient of Variation (%) | 3.3 | 0.3 | 2.4 |
| **Mixed EPS** | 773.673 | 443.82 | 36.661 |
| | 762.243 | 443.54 | 34.951 |
| | 771.14 | 444.03 | 36.101 |
| Mean | **769.018** | **443.796** | **35.904** |
| Standard deviation | 6 | 0.24 | 0.87 |
| Coefficient of Variation (%) | 0.6 | 0.04 | 1.9 |
| **Graphite EPS** | 684.789 | 446.858 | 34.327 |
| | 680.721 | 444.365 | 36.043 |
| | 681.762 | 444.981 | 34.862 |
| Mean | **682.424** | **445.401** | **35.077** |
| Standard deviation | 2.11 | 1.29 | 0.87 |
| Coefficient of Variation (%) | 0.2 | 0.2 | 2.04 |
| **Graphene PS** | 393.109 | 448.21 | 31.502 |
| | 391.273 | 448.02 | 31.368 |
| | 390.879 | 447.94 | 30.748 |
| Mean | **391.753** | **448.056** | **31.206** |
| Standard deviation | 1.19 | 0.138 | 0.402 |
| Coefficient of Variation (%) | 0.2 | 0.02 | 1.05 |

Kinetic parameters have been calculated using the MCC measurements for heat release rate at different heating rates. Thus, each sample was burnt at $40^0$ C, $60^0$, $80^0$ and $90^0$ C, respectively. A graph with 1/T plotted in the x axis and natural logarithm of peak reaction rate for every temperature plotted in the y axis was used to conduct the analysis. The results will give a straight trendline where the activation energy E can be obtained from the slope of the line and the intercept of the y axis represents ln ($\Phi(\alpha)$ A) [55]:

$$ln(r) = ln(\Phi(\alpha)A) - \frac{E}{RT} \quad (4.1)$$

, where r is the peak reaction rate (1/s), $\Phi(\alpha)$ is kinetic function, A represents the pre-exponential factor (1/s), E is the activation energy (J/mol.K), R is the universal gas constant (J/mol K) and T is the temperature (K).

This method can be applied for a single step reaction, but it can be also extended to multi-step reactions by formal representation of a multiple peak curve using MCC as a sum of a single-peak curves. The reaction rate for a single step process can be expressed as:

$$r = A\Phi(\alpha)\exp(-E/RT) \tag{4.2}$$

, where r is the reaction rate (1/s), A is pre-exponential factor (1/s), $\Phi(\alpha)$ is kinetic function with $\alpha$ between 0 and 1, E is the activation energy (J/mol.K), R is the universal gas constant (J/mol K) and T is the temperature of the sample (K).

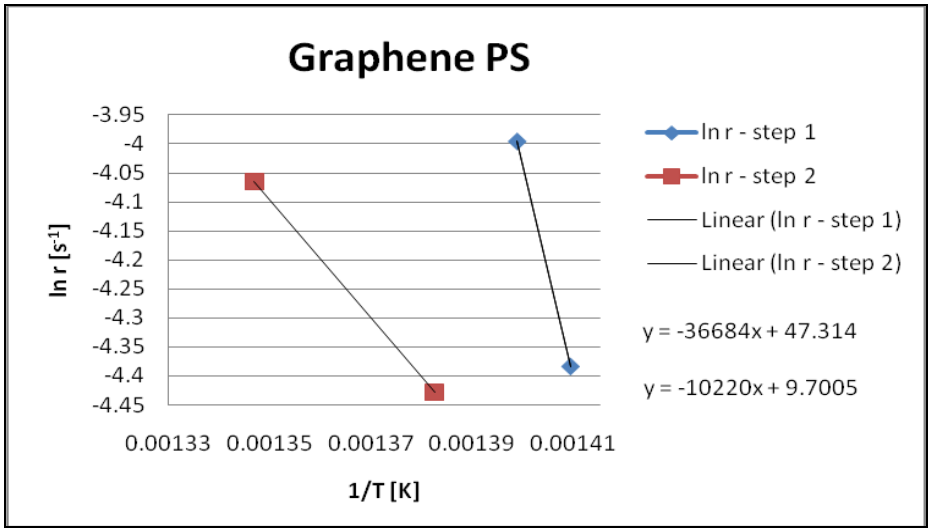


Figure 21 Plot of ln r against inverse of temperature in case of Graphene PS masterbatch experiments

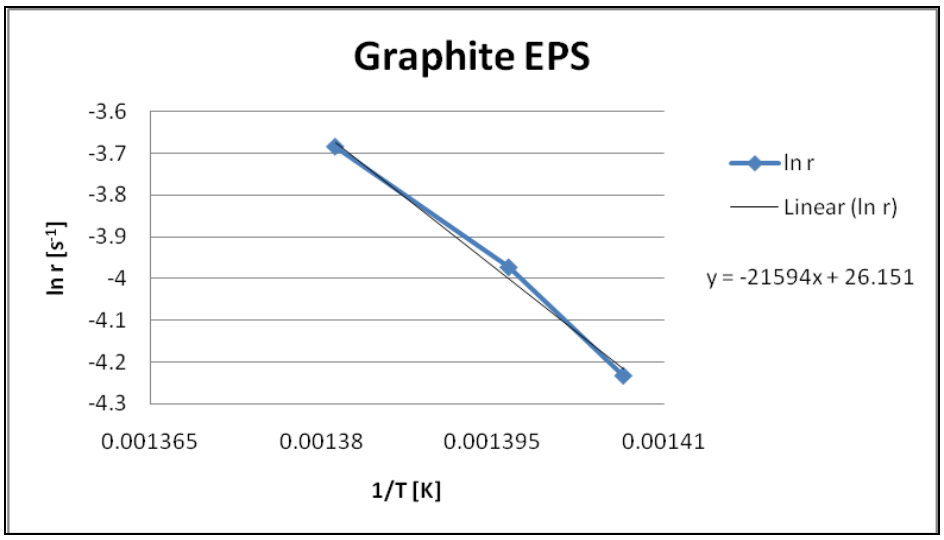


Figure 22 Plot of ln r against inverse of temperature in case of Graphite EPS experiments

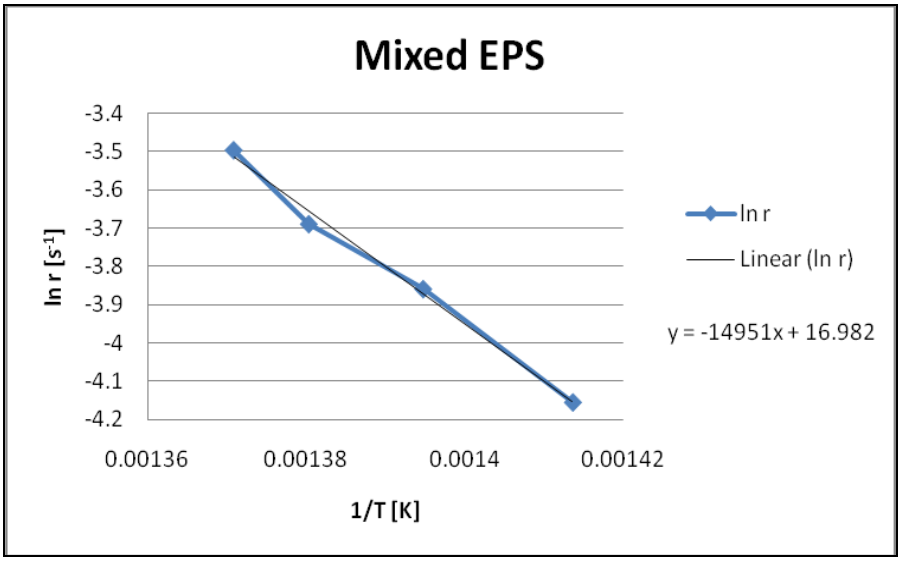


Figure 23 Plot of ln r against inverse of temperature in case of Mixed EPS experiments

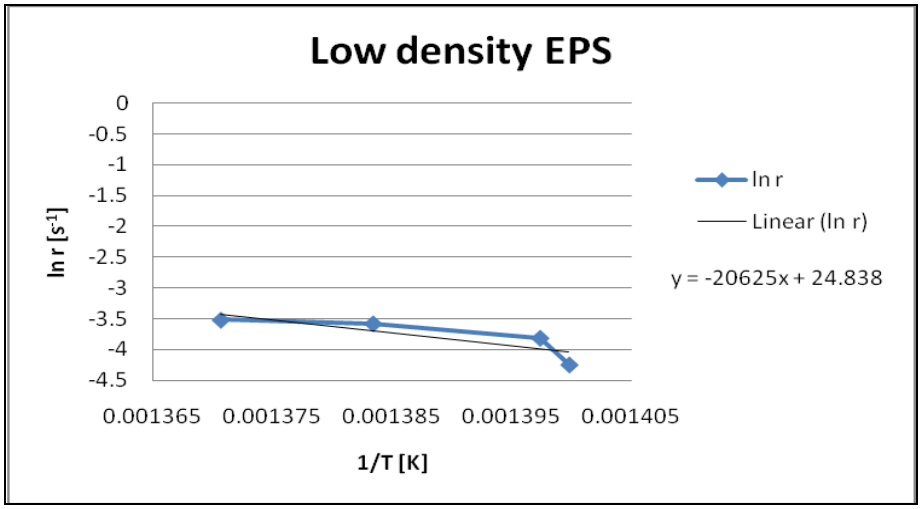


Figure 24 Plot of ln r against inverse of temperature in case of Low density EPS experiments

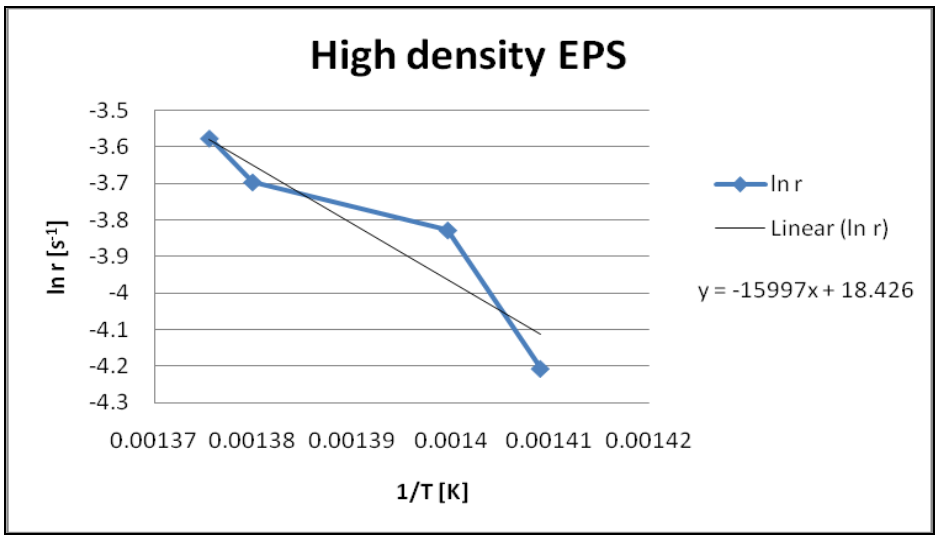


Figure 25 Plot of ln r against inverse of temperature in case of High density EPS experiments

Using the graphs from figure 21 to figure 25 and the equation (4.1), the activation energy is calculated and the results are presented in table 4.

Table 4 Kinetic parameters calculated from MCC measurements

| Material | Density (kg/m$^3$) | E (kJ/mol) | A (s$^{-1}$) |
|---|---|---|---|
| Graphene PS | 911 | 305.1 –step 1<br>84 –step 2 | 3.59E20 –step 1<br>16325 –step2 |
| Graphite EPS | 15 | 179.5 | 6.68E11 |
| Mixed EPS | 15 | 124.3 | 2.49E07 |
| Low density EPS | 15 | 171.4 | 6.65E10 |
| High density EPS | 20 | 133 | 1.03E08 |

In order to calculate the pre-exponential factor, it is necessary to determine the kinetic function $\Phi(a)$ by plotting the dependencies $A\Phi(a) = r(a)exp(-E/RT(a))$ normalized by the $\Phi(1/2)$. An example of this plot for graphite EPS is presented in figure 26.

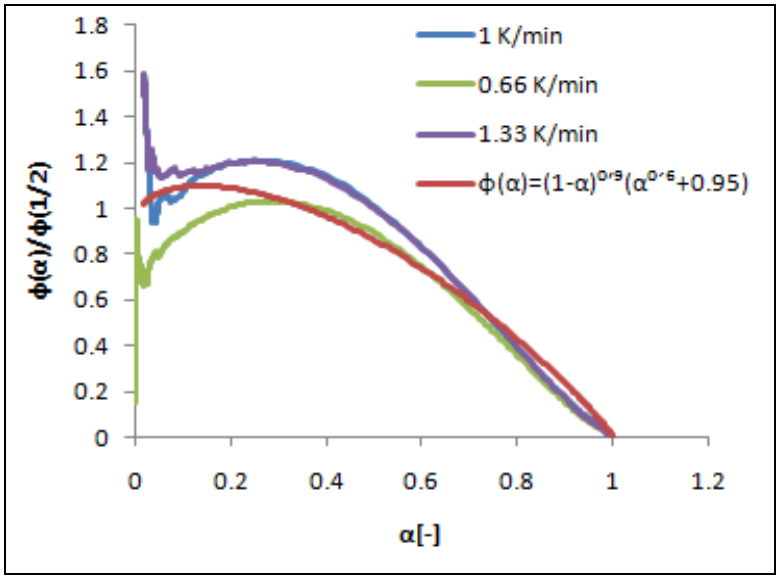


Figure 26 Determination of the kinetic function using dependencies plot

Since the plotted data in figure 26 may have any differences during measurement, the autocatalytic function is used to approximate the kinetic function shape. The red line represents the best fit function, where coefficient values are n=0.9, m=0.6 and $\alpha_0$=0.95. The relation of the autocatalytic function is the following:

$$\Phi(a) = (1-a)^n \cdot \left(a^m + a_0\right) \tag{4.3}$$

The basis of this method is the iso-conversional approach, also known as the model-free method where activation energy is found over a range of conversions if the reaction is a singles step chemical reaction. When the reaction is a single step chemical process the value of activation energy does not vary with conversion, whereas for complex processes activation energy fluctuates with respect to α. All the polystyrene compounds, except graphene PS, investigated during this study have followed the same pattern where the activation energy E did not change substantially, as shown in figure 27. When averaging over the entire range of conversions it was found for graphite EPS that activation energy is around 179 kJ/mol with a standard deviation of 8.5 kJ/mol.

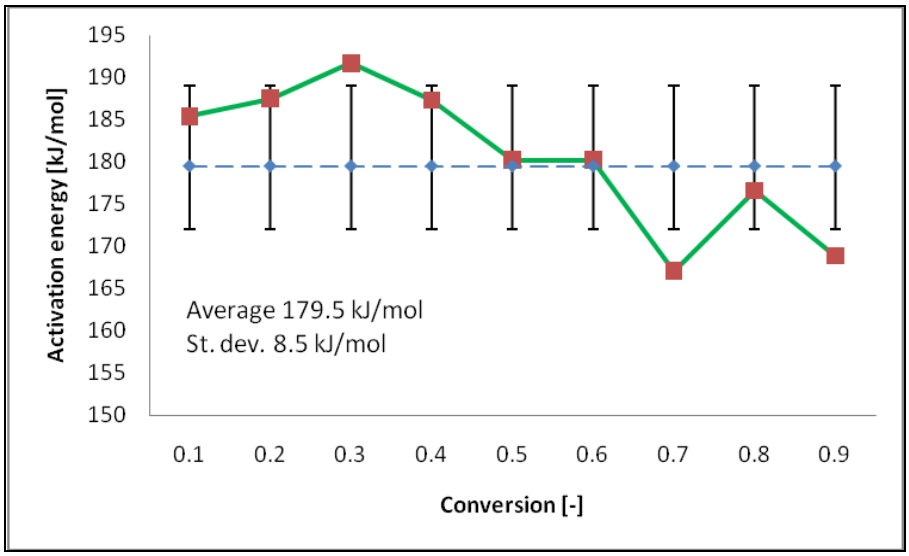


Figure 27 Activation energy values with repect to conversion, α

A graph representing the heat release rate curves for all the polystyrene samples on a $60^0$ C/min heating rate is presented in figure 28.

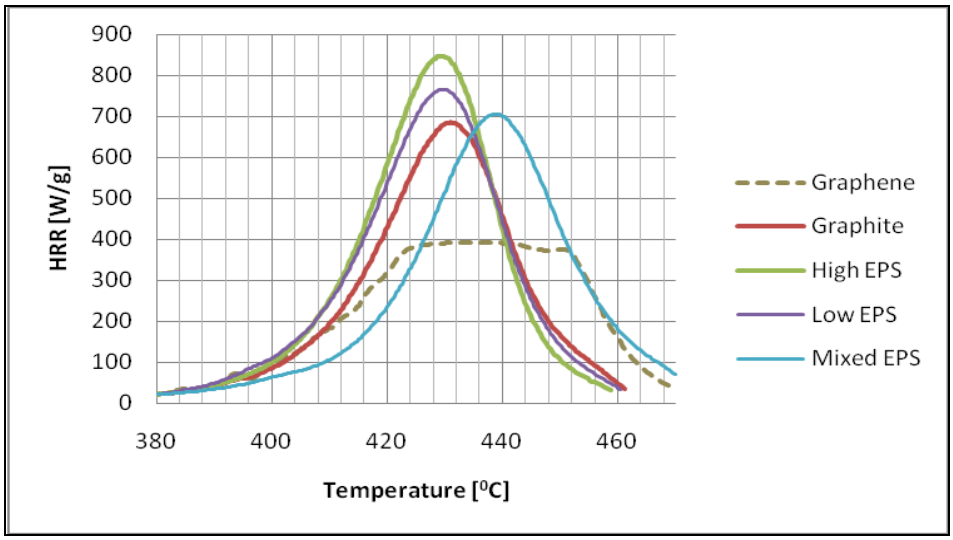


Figure 28 Heat release rate profiles on a $60^0$ C/min heating rate

The maximum value of heat release rate is generated by high density EPS, while the lowest is given by graphene PS mastebatch. This value is almost half the peak obtained for the high density material. Unlike the other compounds, graphene PS reaches a peak around 393 W/g and starts to decay after 440 seconds, but for a short period of time it follows another peak and starts to decay again. This behavior could be explained by the fact that it is a two-step chemical reaction. It first combusts the volatiles from polystyrene and then a char is formed due to the graphene introduction in its structure. In general, the peak temperature where the maximum heat release rate is observed tends to be around $430^0$ C, except mixed EPS for which it is shifted towards $440^0$ C.

## 4.4 Cone Calorimeter measurements

Horizontal samples of 100 x 100 x 10 mm were exposed to a level of irradiance of 35 kW/$m^2$ into the Cone Calorimeter, as shown in figure 29. The ambient temperature during the measurements was $19.6^0$ C and it was kept constant throughout the entire experiment. Additional to the cone heater, a spark igniter was placed above the surface of the specimens. It was observed that in the first stage of heating, all the polystyrene samples melt down very fast and start to produce volatiles and fumes. The onset temperature of the melting point for graphite and graphene PS was delayed compared with other specimens. Immediately after ignition, they burnt with high flames and reached a sharp peak heat release rate and then suddenly start to decrease. The values of heat release rate per unit area may be slightly underestimated as these thermoplastic materials form a liquid pool which goes towards the edges of the aluminum foil inside the sample holder.

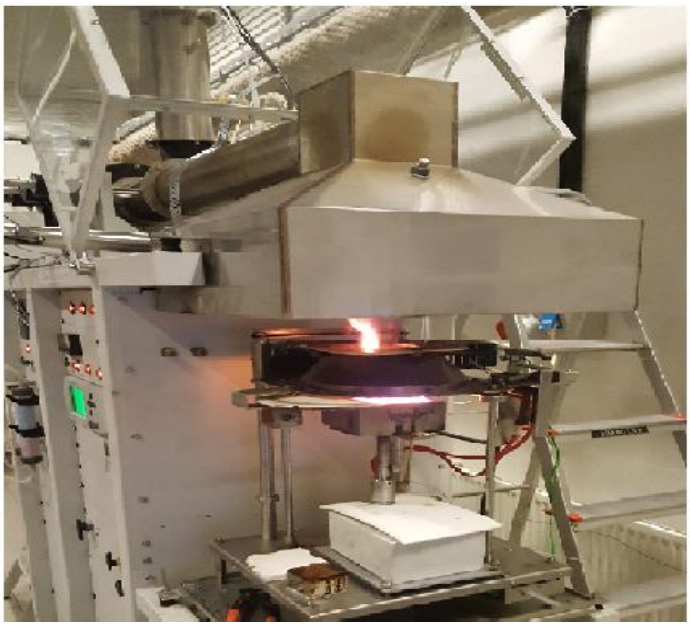

Figure 29 Cone Calorimeter set-up

At the end of the burning stage each sample holder was weighted to determine the amount of residue. The only material that formed a residue was the graphene PS masterbatch which

yielded nearly 3 % char from the initial mass, which corresponds to the amount of graphene added to its composition.

The calculated HRR for the analyzed materials is presented in the figures below.

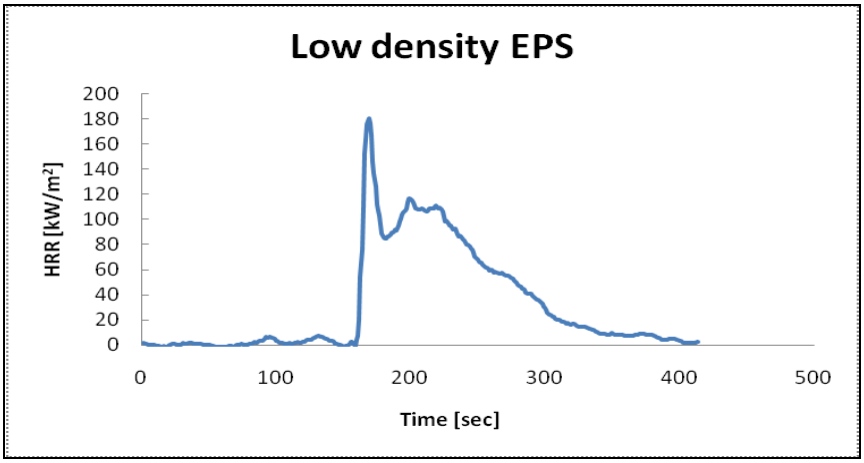


Figure 30 HRR results for low density EPS

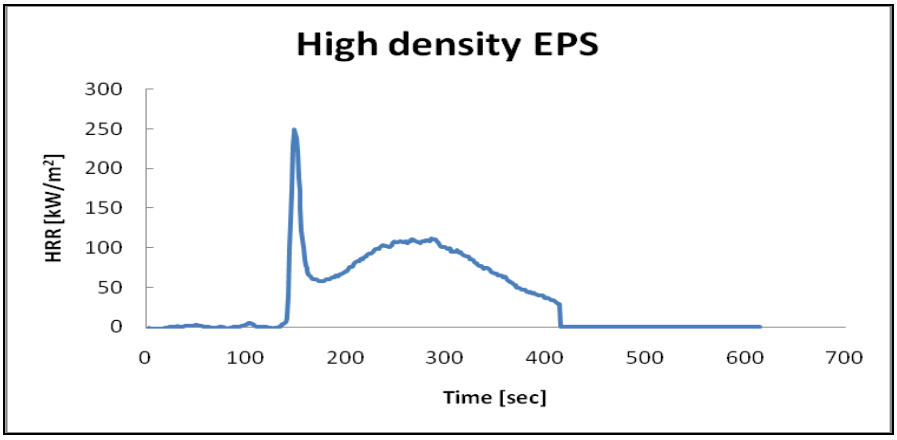


Figure 31 HRR results for high density EPS

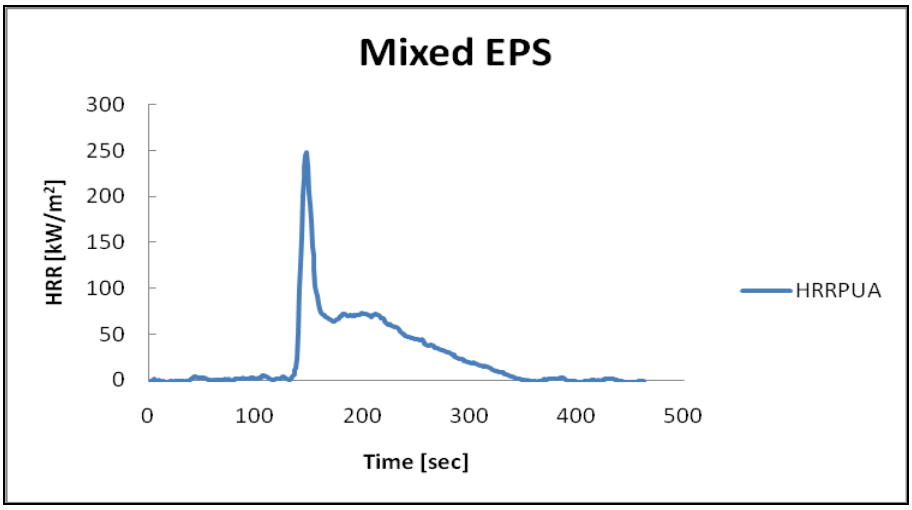


Figure 32 HRR results for mixed EPS

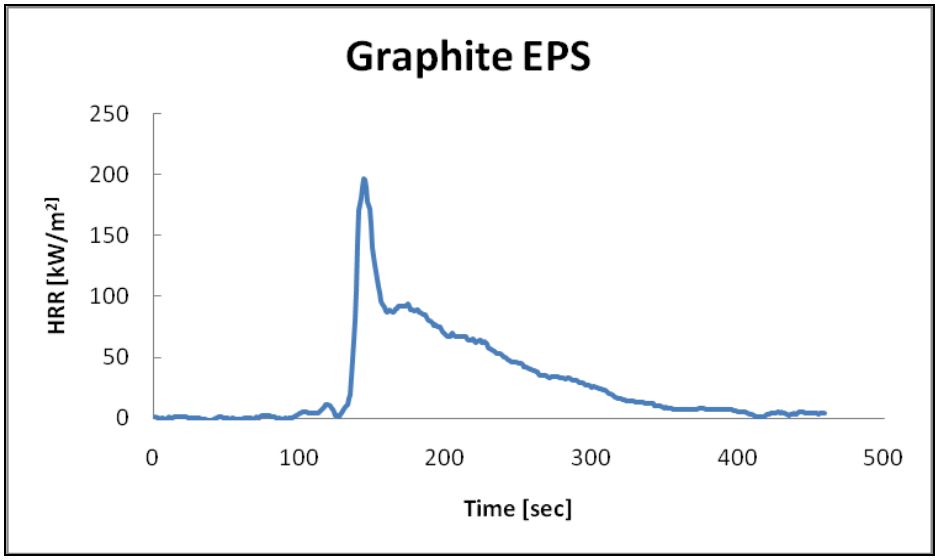


Figure 33 HRR results for graphite EPS

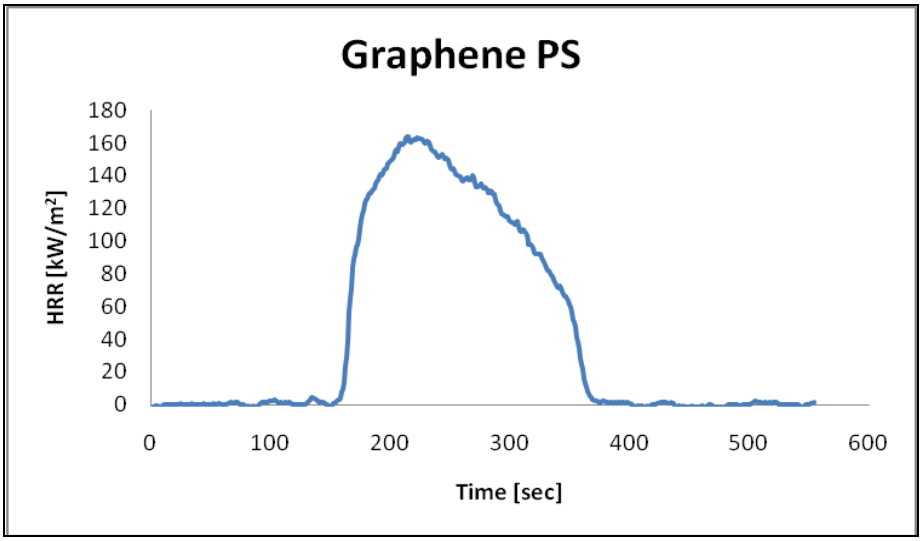


Figure 34 HRR results for graphene EPS

It should be noted that the heat release rate value for graphene PS masterbatch was not determined for the same thickness since this material was in a form of pellets and it may not present a homogeneous structure like expanded graphene polystyrene. There is also a difference in density between raw graphene PS and the final product which may also influence the experimental results. The results presented in figure 34 are obtained for a 6 grams sample which displayed an equivalent burning period like the other expanded polystyrene specimens.

The measured heat release rate per unit area for all the specimens varied between 160 and 250 kW/m$^2$ with the lowest values encountered for low density and graphene EPS. Unlike the results obtained in the MCC, the graphite and mixed EPS showed higher heat release rate values compared to low density EPS.

## 4.5 TGA-DSC measurements

An STA 449 F3 instrument was employed for the determination of the heat of reaction values. This parameter represents the energy required to convert the material into reactant, which is basically the enthalpy difference between the products and the reactant. Thus, all the specimens were placed in $Al_2O_3$ crucibles and exposed on a heating rate of $10^0$ C/min up to $500^0$ C, as it was already expected that the peak temperature will be reached within this interval. All the measurements were performed under purely nitrogen environment.

For the calculation of the heat of reaction, it was first plotted the TGA mass loss curve and the heat flow recorded by the DSC measurement, superimposed on the same graph. Furthermore, it was identified the moment when sample mass loss reaches 10 % difference, both at the beginning and at the end of thermal decomposition stage, as shown in figure 35.

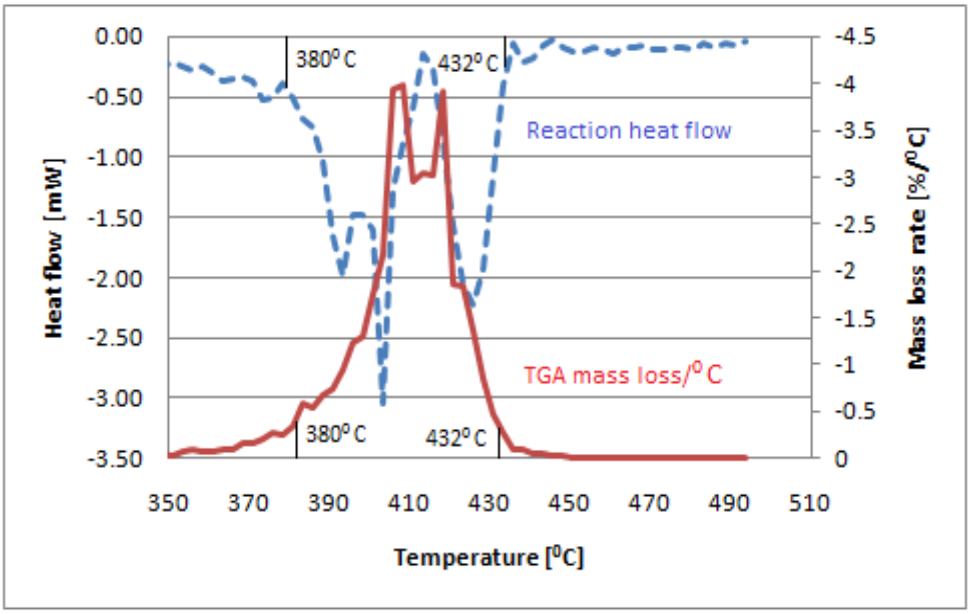


Figure 35 TGA mass loss and reaction heat flow for graphene PS masterbatch

When reaction heat flow shows negative values over the range of interest it means that there is an endothermic reaction that absorbs heat from its environment, as presented in the graph above. Knowing the temperatures where the TGA mass loss is 10 % of the difference between the minimum and maximum values of the specific reaction, then the heat of reaction can be estimated using the following formula [67]:

$$\Delta h_r = \frac{1}{m_0 - m_f} \int_{T_S}^{T_E} \left(\frac{dq}{dt}\right) dT \cdot \frac{dt}{dT} \tag{4.4}$$

, where $m_0$ is the initial mass [g], $m_f$ is the mass after thermal decomposition [g], $\int_{T_S}^{T_E} \left(\frac{dq}{dt}\right) dT$ is the integral of reaction heat flow between selected temperatures, as shown in figure 35.

Since the result of the integration is given in $mW^0C$, the equation requires the multiplication with heating rate applied during experiments (dT/dt) to get J/g.

It can be observed in the figure 35 that graphene PS forms two peaks on the same mass loss rate curve which clearly explains that this material follows two chemical reaction steps. Each peak corresponds to a similar shape in the heat flow curve. There is a small mismatch encountered for Low density EPS where mass loss curve is shifted towards the left side of the graph. This difference has been reported by Pau et al. [67] as an influence of higher heating rate on the sensitive devices of the testing apparatus. TGA-DSC results for the rest of the materials are presented in the Appendix 1.

Similarly, the heat of reaction was estimated for all the materials and the results are given in table 5.

Table 5 Heat of reaction values from TGA-DSC measurements

| **Material** | **Density ($kg/m^3$)** | **Heat of reaction (kJ/kg)** | |
|---|---|---|---|
| | | **Solid** | **Melt** |
| Graphene PS | 911 | 300 | - |
| Graphite EPS | 15 | 850 | - |
| Mixed EPS | 15 | NA | NA |
| Low density EPS | 15 | 32 | 1600 |
| High density EPS | 20 | 90 | 1450 |

The results presented in the table above emphasize two different patterns. The first one, which is characteristic to all the thermoplastic materials, identifies a melting point around $230^0$ C and a corresponding endothermic reaction described by an enthalpy for the solid phase, while for the second behavior encountered with the addition of graphite and graphene in the polystyrene matrix, the thermal decomposition starts in a first stage and the melting point follows this step. This second pattern is in line with observations depicted during the Cone Calorimeter experiments where both graphite and graphene PS showed a delay in the formation of pool fire inside the holding pan.

# 5. FDS SIMULATIONS

## 5.1 Pyrolysis simulation concept used in FDS

Pyrolysis is a fairly complex phenomenon where a thermochemical decomposition of combustible materials occurs at elevated temperatures. As shown in figure 36, heat is transferred from flames to the solid sample through radiation, and thermal decomposition produces combustible volatiles from the solid fuel. In turn, this ensures a heat feedback mechanism to the surface of the pyrolysing material. Therefore, it is necessary to consider a number of processes when pyrolysis modeling is performed [68]:

- heat transfer through solid surface from fire exposure;
- thermal decomposition that produces combustible or non-combustible products;
- mass transfer of oxygen from ambient to the pyrolysis products.

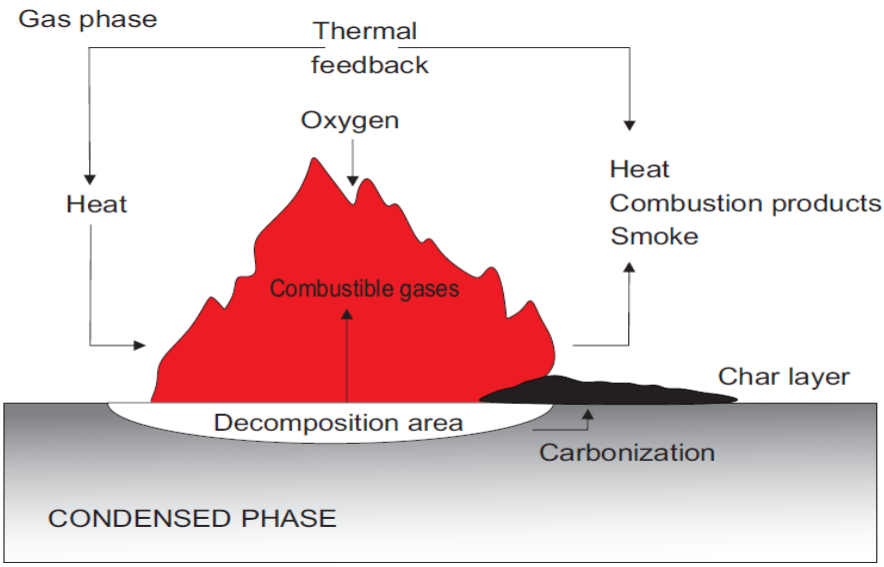


Figure 36 Pyrolysis of a solid fuel (redrawn from [69])

Different comprehensive pyrolysis models have been developed in the recent years. The advantage of these tools is that they can simulate multi-step thermal decomposition reactions and materials with multiple layers that have different decomposition behavior [70]. The general concept of pyrolysis modeling in fire safety engineering involves the evaluation of mass lot rate per unit area as a result of decomposition of a solid phase under fire conditions. Based on the experimental data using small-scale methods, the pyrolysis simulation conducted during this study uses comprehensive models with kinetics, where an Arrhenius type expression is involved to model the reaction.

The rate constant as function of temperature may be expressed as follows:

$$k_f = AT^{\beta} e^{-E/RT} \tag{5.1}$$

, where $k_f$ is the rate constant ($s^{-1}$), A is the pre-exponential factor ($s^{-1}$), T is the temperature (K), E is the activation energy (kJ/mol), R is the universal gas constant (kJ/molK).

According to the FDS Technical reference Guide the one-dimensional heat conduction for solid phase is computed using the following formula [71]:

$$\rho_s c_s \frac{\partial T_s}{\partial t} = \frac{\partial}{\partial x}\left(k_s \frac{\partial T_s}{\partial x}\right) + \dot{q}_s''' \tag{5.1}$$

, where the source term $\dot{q}_s'''$ contains the chemical reactions and radiative absorption.

Taking the boundary conditions x=0 at the surface of the material, then

$$\left(-k_s \frac{\partial T_s}{\partial x}(0,t)\right) = \dot{q}_c'' + \dot{q}_r'' \tag{5.2}$$

, where $\dot{q}_c''$ is the convective and $\dot{q}_r''$ is the radiative heat flux. The convective part is obtained separately for DNS and LES, but since the computational capabilities do not allow a DNS approach, it will be calculated using the next correlation:

$$\dot{q}_c'' = h\left(T_g - T_W\right) \tag{5.3}$$

, where $T_g$ is the gas temperature of the nearest gas-phase cell.

The net radiative heat flux is the sum of incoming and outgoing components

$$\dot{q}_{r,in}'' = \varepsilon \int_{s' n_w < 0} I_w\left(s'\right)\left|s' \cdot n_w\right| d\Omega \tag{5.4}$$

$$\dot{q}_{r,out}'' = \varepsilon\sigma {T_w}^4 \tag{5.5}$$

Substituting the relation 5.3. and 5.5. in equation 5.2., the heat transfer becomes

$$\left(-k_s \frac{\partial T_s}{\partial x}(0,t)\right) = h\left(T_g - T_s(0,t)\right) + \left[\dot{q}_{r,in}'' - \varepsilon\sigma {T_w}^4\right] \tag{5.6}$$

Both conductivity and volumetric heat capacity of the solid are defined as

$$k_s = \sum_{a=1}^{N_m} X_a k_{s,a} \qquad \rho_s c_s = \sum_{a=1}^{N_m} \rho_{s,a} c_{s,a} \tag{5.7}$$

, where $N_m$ is the number of material components forming the solid material, while $X_\alpha$ is the mass fraction of component α and $\rho_{s,\alpha}$ is the component density equal to the product between the density of the composite material and the mass fraction of each component, $\rho_\alpha Y_\alpha$. The volume fraction of component α is generated using the next relation:

$$X_a = \left( \frac{\frac{\rho_{s,a}}{\rho_a}}{\sum_{a=1}^{N_m} \frac{\rho_{s,a'}}{\rho_{a'}}} \right) \tag{5.8}$$

, where $\rho_\alpha$ is the density of material α.

The chemical source in the heat conduction equation is defined as

$$\dot{q}_{s,c}'''(x) - \rho_s(0) \sum_{a=1}^{N_m} \sum_{\beta=1}^{N_{r,a}} r_{a\beta}(x) H_{r,a\beta} \tag{5.9}$$

, where $r_{\alpha,\beta}$ is the reaction rate for the βth reaction of the αth material component and $H_{r,\alpha\beta}$ is the corresponding heat of reaction.

The local density of material component α is modified over the time according to the solid phase species conservation equation

$$\frac{\partial}{\partial t}\left( \frac{\rho_{a,s}}{\rho_s(0)} \right) = -\sum_{\beta=1}^{N_{r,a}} r_{a\beta} + S_a \tag{5.10}$$

For homogeneous reaction the decomposition rate for a material undergoing one or more reactions is calculated as follows

$$r_{a,\beta}(x) = A_{a\beta} \left( \frac{\rho_{s,\beta}(x)}{\rho_s(0)} \right)_{s,a}^{n_{s,a\beta}} exp\left( -\frac{E}{RT_s(x)} \right) \tag{5.11}$$

, where $r_{\alpha\beta}$ is the reaction rate for βth reaction of the αth component, $\rho_{\alpha,s}$ is the transient mass concentration and $\rho_s$ (0) is the initial density of the layer. The first term in the right is the reactant dependency and the second one represents the Arrhenius function.

## 5.2 MCC numerical simulations

Despite the iso-conversional method used in the previous chapter, the Arrhenius parameters can be estimated from the data generated by the FDS simulation. The reaction rate at which chemical process is developed may be calculated using the following formula:

$$r_{a,p} = \frac{\dot{q}}{\left( \frac{1}{\beta} \int_{T_0}^{\infty} \dot{q}(T) dT \right)} \tag{5.12}$$

, where $\dot{q}$ is the specific heat release (kJ/g) and β is the heating rate ($^0$C/min).

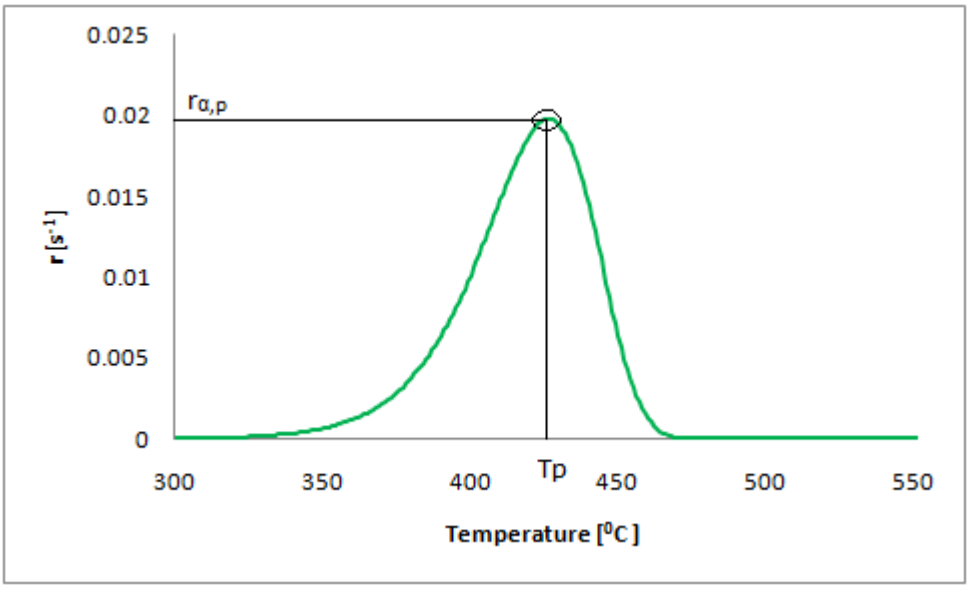


Figure 37 Plot of reaction rate dependence with temperature

From figure 37, the peak reaction rate and the corresponding temperature could be extracted. Once these two values are known, the activation energy may be evaluated using the following equation:

$$E_a = RT_{a,p}^2 \frac{A_a}{\beta} exp\left(-\frac{E_a}{RT_{a,p}}\right) \approx \frac{RT_{a,p}^2}{\beta} \cdot \frac{er_{a,p}}{Y_{a,0}} \tag{5.13}$$

Then $A_\alpha$ can be directly estimated from equation 5.11.:

$$A_a = \frac{r_{a,p}}{Y_{a,p}} exp\left(\frac{E_a}{RT_{a,P}}\right) \approx \frac{er_{a,p}}{Y_{a,0}} exp\left(\frac{E_a}{RT_{a,P}}\right) \tag{5.14}$$

, where $Y_{\alpha,0}$ and $Y_{\alpha,P}$ are the mass fraction at the beginning of the pyrolysis and when the heat release rate reaches its peak, respectively.

Table 6 Kinetic parameters calculated from MCC simulation

| Material | Density (kg/m$^3$) | E (kJ/mol) | A (s$^{-1}$) |
|---|---|---|---|
| Graphene EPS | 911 | 152.1 | 5.8E9 |
| Graphite EPS | 15 | 228.84 | 2.66E15 |
| Mixed EPS | 15 | 252.94 | 1.79E17 |
| Low density EPS | 15 | 267.62 | 2.1E18 |
| High density EPS | 20 | 260.73 | 7.3E17 |

In general, kinetic parameters values calculated with FDS simulation, as shown in table 6, tend to be higher than those obtained with the iso-conversional approach. In order to get more accurate results an optimization study should be performed. Either the well-known genetic algorithm or the classic trial-and-error method can be used. Although the peak heat release rate values are close to the experimental ones as shown in figures below, kinetic parameters are very sensitive to small changes in reaction rate. Therefore, thoroughly analysis should be employed when these reaction parameters are calculated using simulation methods.

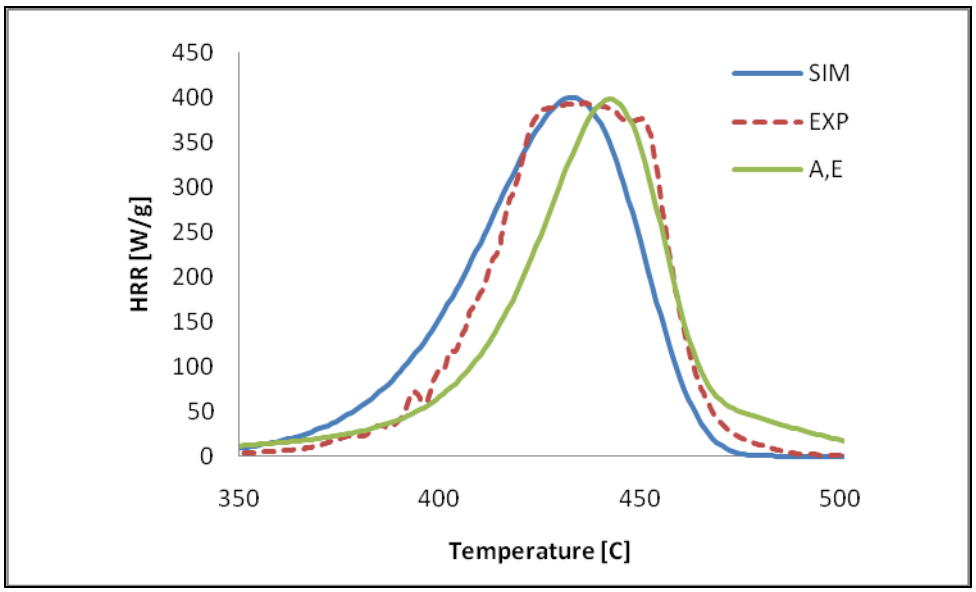


Figure 38 MCC simulation for graphene PS

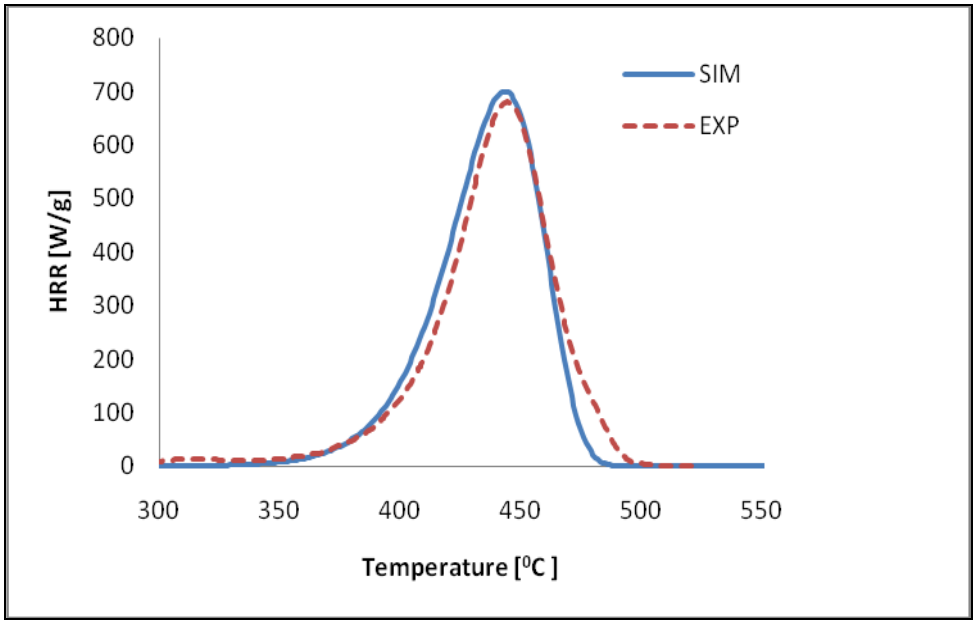


Figure 39 MCC simulation for graphite EPS

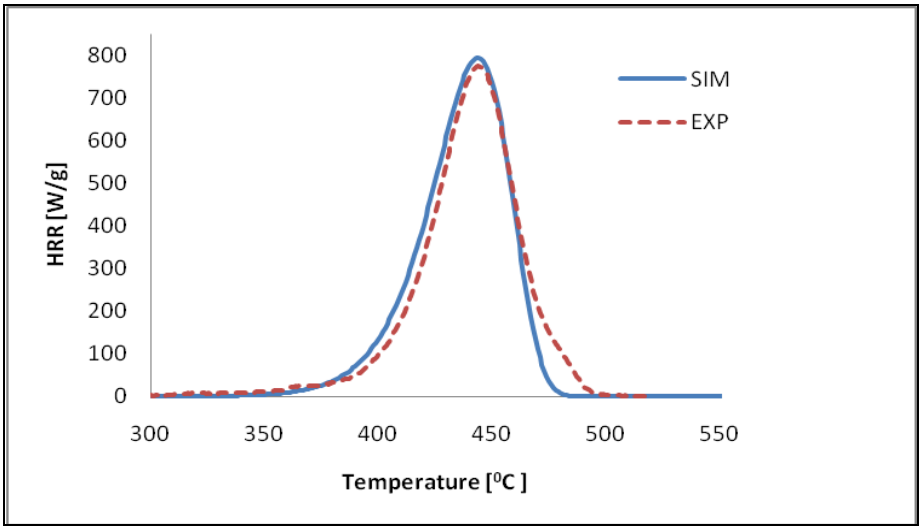


Figure 40 MCC simulation for mixed EPS

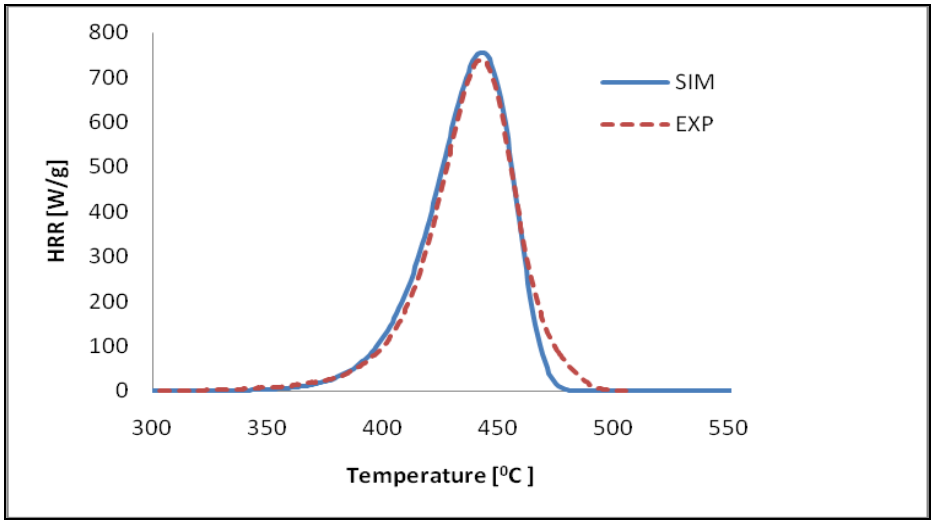


Figure 41 MCC simulation for low density EPS

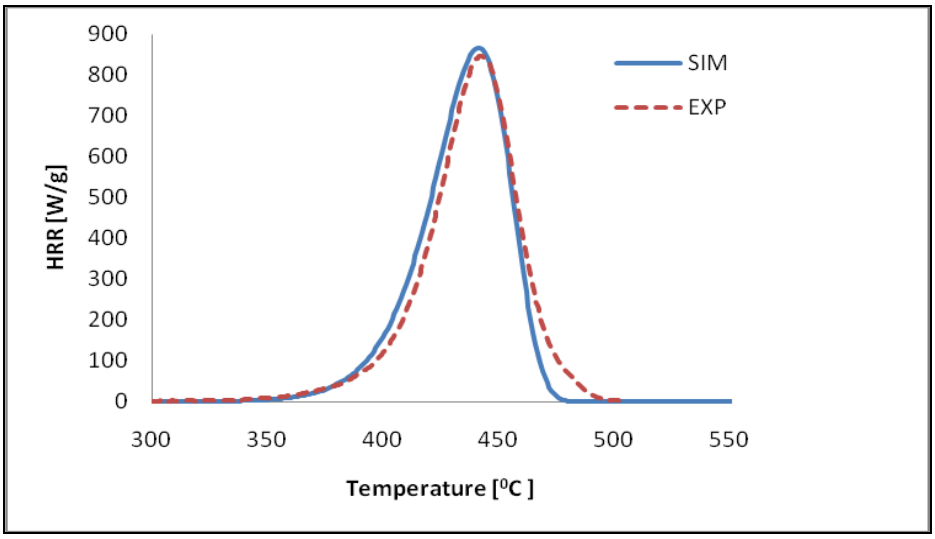


Figure 42 MCC simulation for high density EPS

Peak error for heat release rate between simulation and the experiments do not exceeds 3 % and the simulation graph follows the same pattern shown in the MCC. There is a small overestimation on the growth phase and a much bigger difference at the end of the decay stage. The simulated curve for graphene PS shows the biggest error in the decay which may be explained by the fact that it undergoes two chemical reactions. By contrary, when only kinetic parameters values are used, instead the reference rate and the corresponding temperature, the decay phase is very well replicated, but the growth part is underestimated. Moreover, the peak of the second reaction is not predicted during the simulation.

## 5.3 Large-scale FDS model

### 5.3.1 Validation study – Zagreb experiment

Two series of large-scale experiments in accordance with BS 8414-1 requirements have been performed in Zagreb, Croatia in March 2014 and May 2014, respectively. The aim of this extensive experimental study was to investigate the fire performance of different thermal insulation composite systems with expanded polystyrene using an external rendering layer.

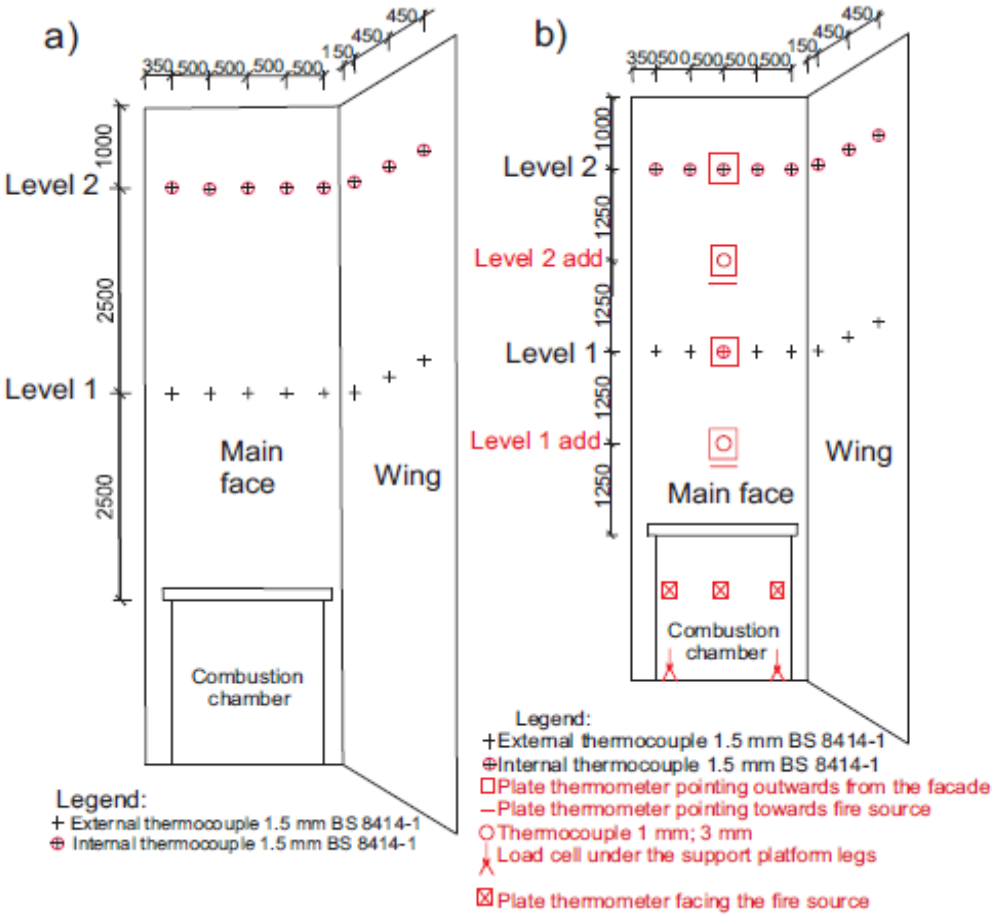


Figure 43 Front view with: a) thermocouples required by BS 8414-1 and b) additional external thermocouples used during the study (redrawn from [72])

Three façade systems were tested during each experiment on different rigs. The experimental set-up was constructed in open air with an L-shaped design. It was 8 m high, with a front wall of 2.6 m wide and a re-entrant corner forming the return wall that extended 1.5 m in front of the combustion chamber. This particular shape was intended to resemble a part from a building corner [73]. The instrumentation used during this study included eight type K thermocouples with 1.5 mm bead diameter on each wing of the specimen. The position of the thermocouples was in conformity with the standard recommendations on two separate levels at 2.5 and 5 m from the top of the combustion chamber. Each series of tests was done with some modifications implemented to the standard. Thus, there were additional plate thermocouples placed at 0.5 m in front of the fire place and 1.25 m above the wood crib enclosure, as shown in figure 43.

The square opening of the combustion chamber had a side length of 2 m were a fire source made of wood cribs was placed in order to produce a nominal heat output of 4500 MJ over 30 minutes at a peak of 3±0.5 MW. The total weight of wood crib varied between 357 and 445 kg and the mass loss of fuel during the burning process was weighted with an electronic load cell. Both series of tests were conducted in the same layout with similar materials, except the weather conditions as the experiments were organized in open air. In the first research the air temperature was close to $15^0$ C and the wind speed ranged between 2 and 5 m/s. For the second trial the outside temperature increased to $25^0$ C, while the wind speed was little less than 2 m/s. Since the atmospheric conditions were slightly different from one test to another, it was observed that burning rate of fuel was much faster in March 2014 when wind had blown with higher speed [73].

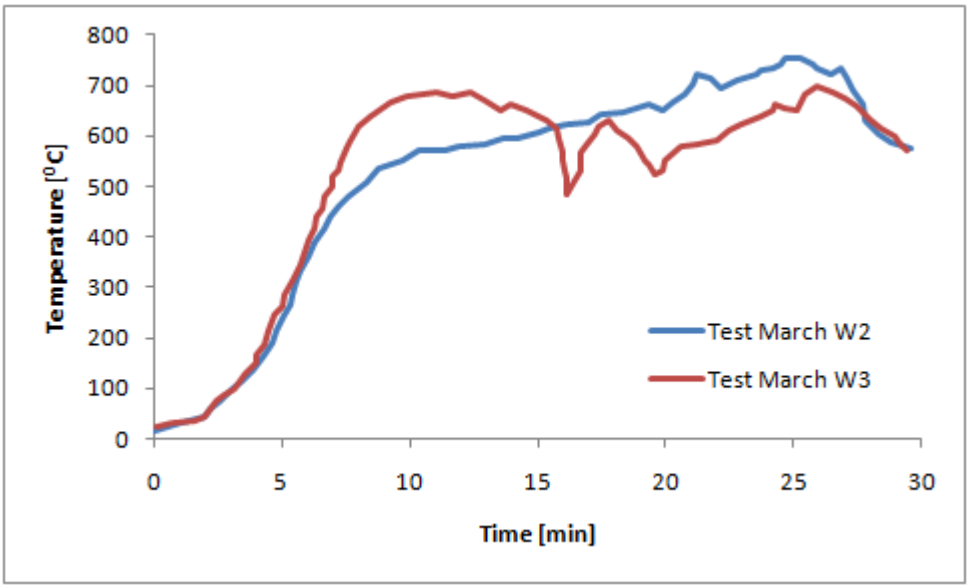


Figure 44 Mean plate thermocouple temperature
recorded at 0.5 m from the combustion chamber (redrawn from [73])

The results of the additional plate thermocouples which were pointing towards the fire are presented in figure 44. As noted by the research team, the measurements were closely

correlated to the fuel consumption since wind effects seemed to increase the temperatures recorded on the plate thermometers [73].

### 5.3.2 Grid sensitivity analysis

Using the experimental data presented in chapter 4 and the validation study from Croatia, a series of two simulations with low density expanded polystyrene and graphene PS were performed. These studies were computed with Fire Dynamics Simulator version 6.7.1. which is a CFD program developed by National Institute of Standards and Technology (NIST) and Technical centre of Finland (VTT). Before the definition of the input parameters for the simulation, the following assumptions were taken into consideration:

- no radiation analysis was performed for this study. The number of radiation angles used was the default 100 from the FDS software;
- the wind effect was not considered. During the validation study the wind blew with speeds up to 5 m/s;
- wood crib was burnt in a form of cubic fire source without taking into account the radiation between each stick from the crib;
- the heat release rate followed a linear ramp of 660 seconds and then reached a steady-state with a peak value of 3400 kW according to data presented in figure 45 (adapted from [73]);
- since the heat release rate gets a steady-state after 11 minutes, the entire simulation was run for only 900 seconds;

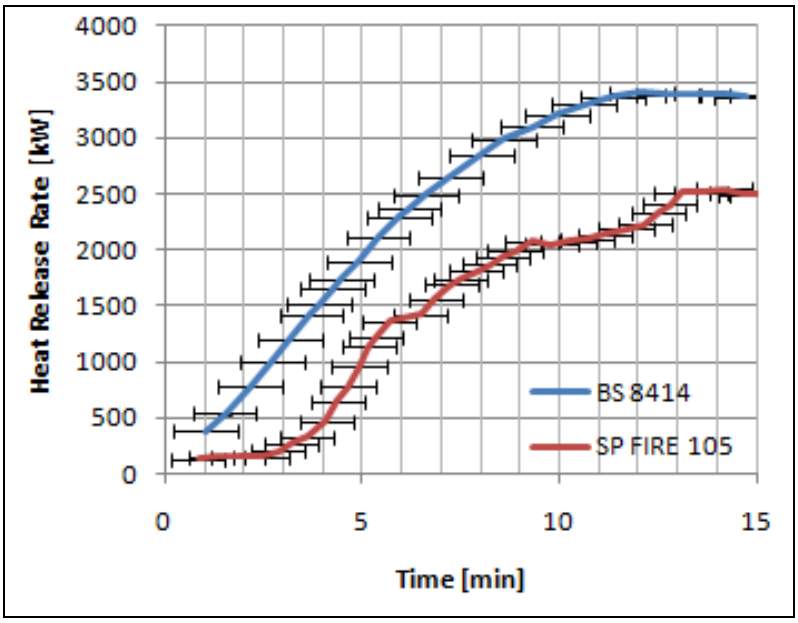


Figure 45 Heat release rate used in the simulations in a comparative study, including BS 8414 set-up

As defined in the FDS User's Guide [5], to describe the evolution of the fire, this software solves numerically Large Eddy Simulation (LES) form of the Navier-Stokes equations. For this reason the finest mesh is the best option to get results close to reality. To define a proper mesh size that gives a reasonable computational time, the non-dimensional relationship

D*/dx was used. In this case, the analysis is for a buoyant plume, and the following equation is used to calculate the value for D*:

$$D^* = \left( \frac{\dot{Q}}{\rho_\infty c_p T_\infty \sqrt{g}} \right)^{2/5} = 1{,}563 \qquad (5.1)$$

, where $D^*$ is the characteristic fire diameter, $\dot{Q}$ is the total heat release rate (3400 kW), $\rho_\infty$ is the ambient density (1.225 kg/m$^3$), $c_p$ is the heat capacity (1.007 kJ/kgK), $T_\infty$ is the ambient temperature (288 K) and g is the gravitational constant (9.81 m/s$^2$).

Additionally, important part of the FDS calculation uses a Poisson solver based on Fast Fourier Transforms (FFTs) in the y and z directions. This means that the second and third dimensions of the mesh should each be of the form $2^l 3^m 5^n$, where l, m and n are integers. Thus, for the 12 m height of the testing rig, some of the most appropriated cell sizes are: 0.30 m, 0.1 m, and 0.05 m. These give a number of divisions equal to 40, 120 and 240 respectively, which can be factored down to the integer numbers mentioned above.

Then, with the selected cell sizes, D*/dx was calculated. According to the FDS User's Guide, a suggested interval for this value is 4<D*/dx<16, which has been used by U.S. Nuclear Regulatory Commission in a series of experimental studies. The next table shows the grid resolutions intended for the sensitivity analysis.

Table 7 Mesh size for the sensitivity analysis

| **Grid Resolution** | **δx** | **D*/δx** |
|---|---|---|
| Coarse | 0.2 | 7.815 |
| Medium | 0.15 | 10.42 |
| Fine | 0.1 | 15.63 |

During this analysis study the temperature and gas velocity values were investigated. This evaluation was performed on the middle axis of the wall containing the combustion chamber at 1.9, 3.25, 4.5 and 7 m from the ground along the z-axis. In addition to the thermocouples required by the standardized method, there were placed another four velocity measurement devices to evaluate the gas speed at the same locations as for the temperature. Since the simulation results showed a steady-state pattern after 11 minutes, the evaluation was performed for an average value of the interest parameters for the last 50 seconds. A numerical scheme is said to be consistent if the discretized equations recover the partial differential equations of interest as dx and dt tend to 0. In the same time the convergence theorem states that if a scheme is both consistent and stable the numerical solution of the discretized equation will converge to the exact solution of the partial differential equations as both dx and dt tend to 0. Analyzing the graphs from the figure 46

and 47, one may conclude that a cell grid of 10 cm tends to be more accurate as final results are much closer to the experimental values.

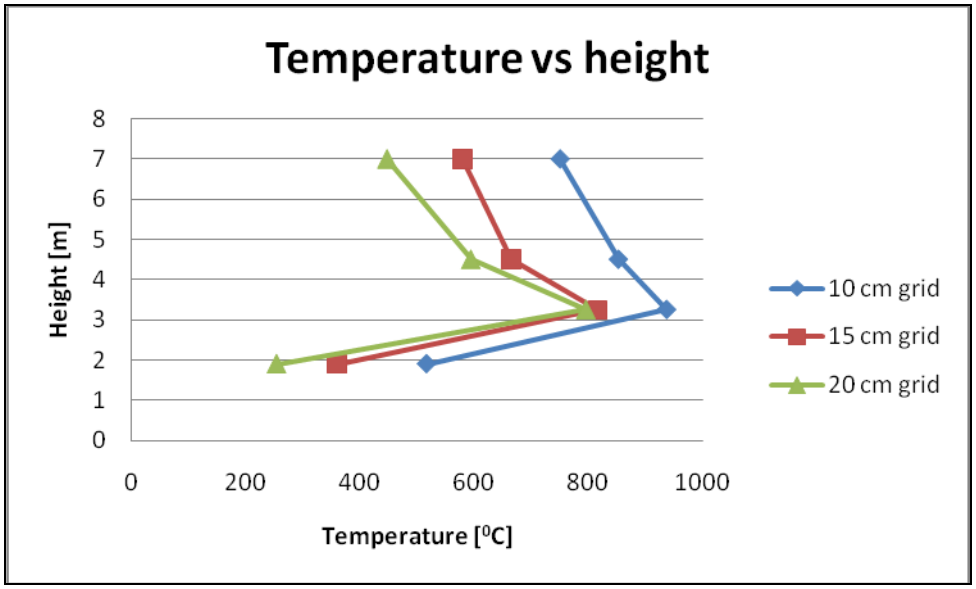


Figure 46 Temperature profiles for different mesh size

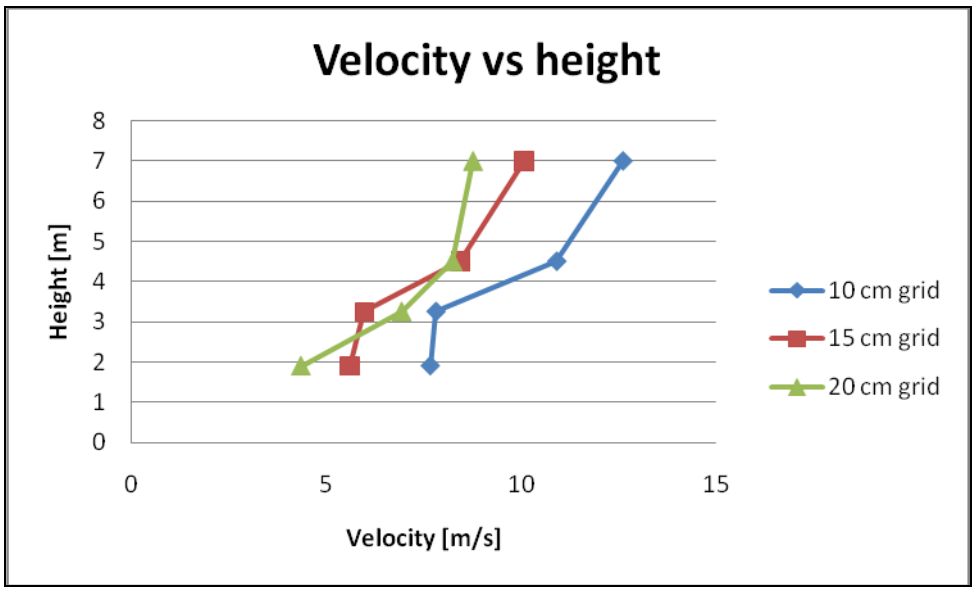


Figure 47 Gas velocity profiles for different mesh size

Moreover, the thermocouple temperatures recorded at 0.5 m in the front of the wood crib seem to be close to the experimental results for the 10 cm grid simulation (figure 48). There is an overestimation during the growth phase, but as soon as the heat release reaches a steady-state, the temperatures calculated during the simulation follow the same pattern with the ones encountered in the large-scale study.

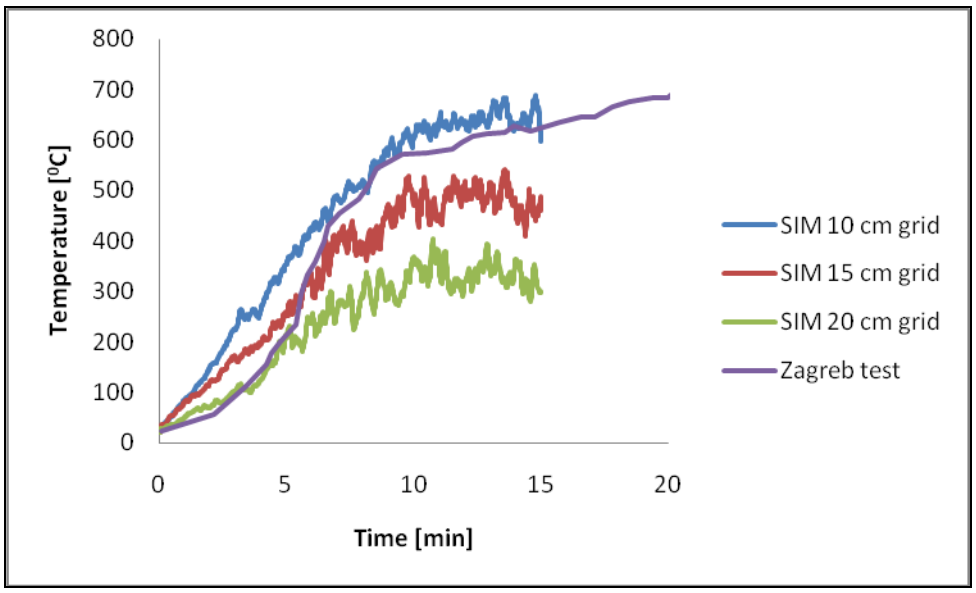


Figure 48 Temperature profile at 0.5 m in front of the combustion chamber

### 5.3.3 Numerical study for large-scale experiment

The purpose of this numerical study is to qualitatively evaluate the temperatures for a façade fire on a testing rig according to BS 8414 requirements. Two numerical simulations for an expanded polystyrene and graphene PS will be performed under the same conditions as presented in the Zagreb experiment.

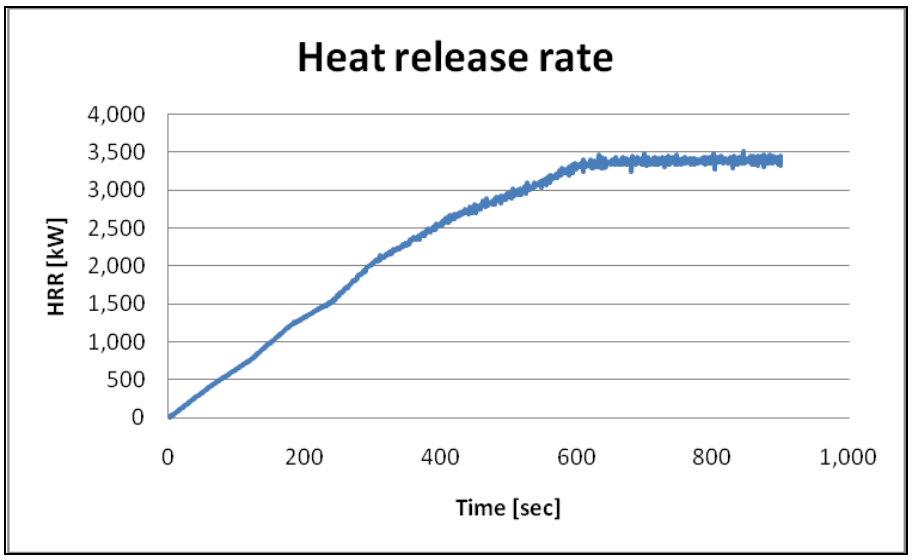


Figure 49 Heat release rate used for the simulations

Each façade test is intended to assess a polystyrene insulating layer without any additional cover or rendering substrate. In all the EIFS systems the insulating material in protected by different materials against weather effects, but the intention of this study is to create a worst case situation where due to ageing or constructive flaws the entire system may behave as a raw polystyrene insulation. Therefore, the heat release rate values for

polystyrene, used in the simulation where taken from the experimental measurements carried with the Cone Calorimeter and ramped accordingly. As part of the limitations subjected to this study, the probed specimen orientation in the Cone Calorimeter was horizontal with a lower level of irradiance than the one expected according to the BS 8414 procedure. The minimum level of irradiance during the calibration of the fire source expected should be 60 kW/m$^2$, compared with only 35 kW/m$^2$ used during the experiments. This hypothetical scenario was created to represent a vertical flame spread of an external fire and to qualitatively evaluate the temperatures recorded during the simulation.

Heat release rate input for wooden crib in both simulations is presented in figure 49 and it is under the standardized requirements where there is allowed a ±0.5 MW fluctuation from the nominal value. Ignition temperature for both materials was taken as the onset of the thermal degradation resulted from the MCC measurements.

### 5.3.4 Simulation results for the large-scale model

During the simulation progress, temperatures were measured at two different levels as stated by the standard. All the thermocouples were placed in accordance with the figure 43 and their values are presented in the figures below.

First level devices may be identified as THCP, while those placed in the upper level are referred as THUP, followed by a number, from 1 to 5 which corresponds to the mounting position, starting from the right side near the re-entrant corner, continuing to the far left of the main wall.

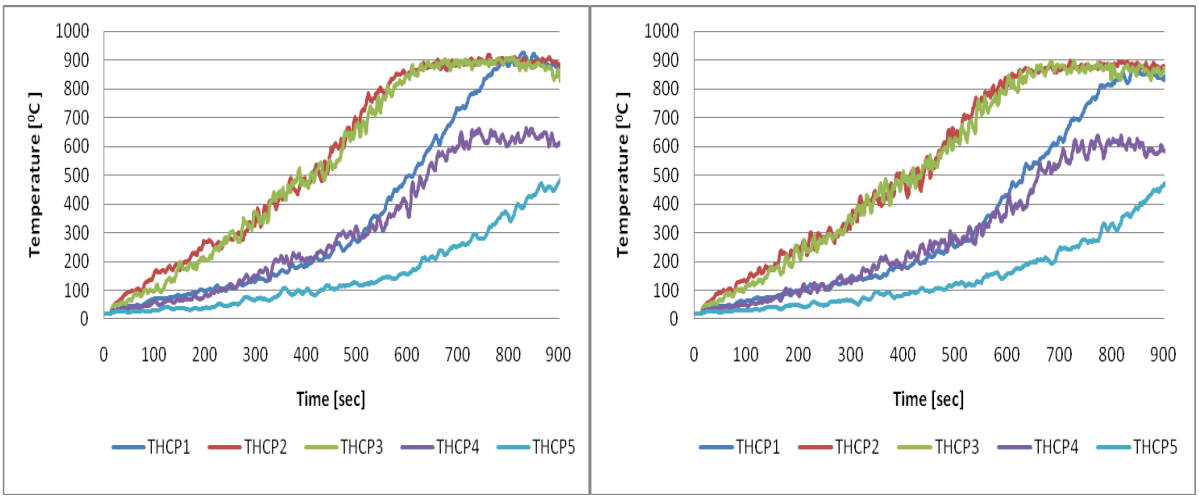


Figure 50 Temperature values at first level: left – low density EPS; right – graphene PS

The accuracy at which temperature is measured during the experiments depends on the instrumentation devices. Hence, the thermocouples embedded into the simulations replicate the experimental conditions. The maximum temperatures are observed in the vicinity of the re-entrant corner where due to radiation from the wing the heat feedback is increased.

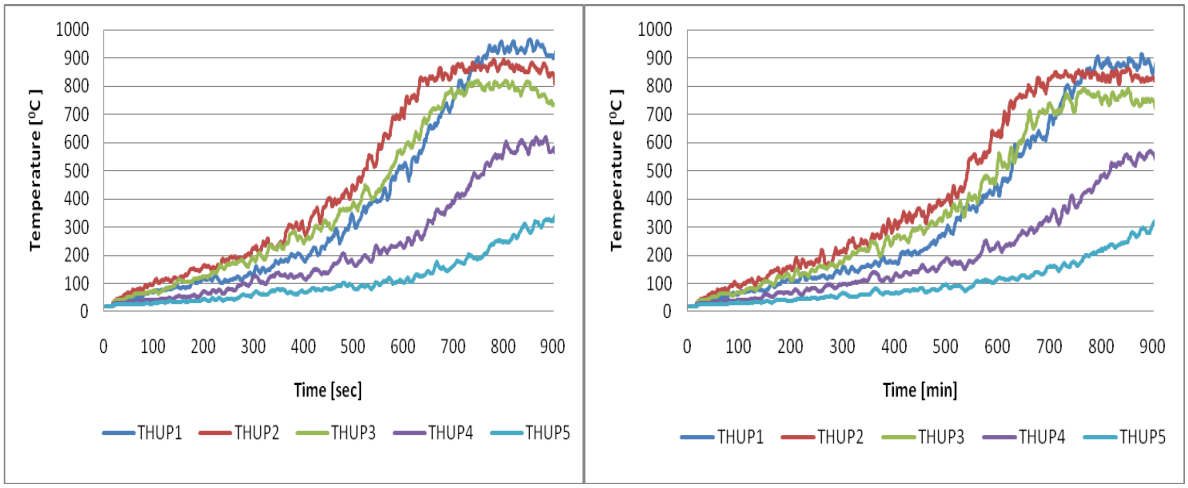


Figure 51 Temperature values at second level: left – low density EPS; right – graphene PS

This effect is more pronounced in the first half of the main wall and it gets lower and lower towards its left edge. Overall values are lower for the graphene PS since the heat release rate per unit area is with 20 kW/m$^2$ smaller compared to the expanded EPS. Nevertheless, the temperatures are sensitive to the heat release rate input in the simulations and an accurate estimation is hard to get for the vertical flame spread using bench-scale methods.

# 6. DISCUSSIONS AND CONCLUSIONS

Fire safety concept of facades has been a long debated issue over the past decades. Not only the fire propagation mechanism is one of the important factors, which makes the evaluation of the external systems very difficult, but also the various range of combustible materials from their structure. Due to energy efficiency requirements there is a considerable controversy between fire safety engineers on one hand and environmental activists on the other. Since most of the thermal insulating materials are combustible and non compliant with safety regulations, they have been proven to be a reliable solution in a world striving for a better environment. Hence, the development of new insulating materials with enhanced flammable properties could be a good alternative to fulfill both legislative requirements.

Based on general results for flammability characteristics depicted from experimental studies, carried with small-scale and bench-scale testing instruments, this study provides a quantitative assessment for various types of polystyrene specimens which may be used as an insulating layer in the external system of the building facades.

In the preliminary stage, all the materials were tested using a Microscale Combustion Calorimeter which requires nanoscale samples in the order of a few milligrams. Samples were first pyrolised and then combusted in a controlled atmosphere with pure nitrogen. Quantitative comparison at different heating rates shows important improvements in the results, when graphene is introduced in the polystyrene matrix. Heat release rate values are considerable reduced as a primary effect of graphene barrier created during pyrolysis. This newly developed emerging material has started to be used with great success for general electronic applications, sensor and imaging and it seems to be a good solution for the fire safety properties of building materials.

Similar results were reported by Bao et al. in a study related to fire safety applications of polystyrene [75]. They investigated expanded polystyrene with graphene up to 2 % in its structure, using Cone Calorimeter and TGA results. Unlike this previous study, the onset temperature of the thermal degradation for graphene PS masterbatch, evaluated in the present report, was only slightly improved compared with the other expanded polystyrene specimens. This small difference is assumed to happen for the graphene PS due to the non-homogeneous structure of the pellets.

Another important behavior is reflected in the MCC heat release rate curves, where it was found that the addition of graphene forms two protuberances on the same curve, while the other polystyrene samples have only one. This observation is in a good agreement with the TGA mass loss rate curves, where graphene PS presents two distinct peaks corresponding to different chemical reaction steps. Unlike the expanded polystyrene materials, this raw graphene PS undergoes two chemical reaction steps as follows:

R1: virgin material ⟶ volatiles + active component

R2: active component ⟶ volatiles + residue

In the next stage, kinetic parameters for all the polystyrene samples were estimated using the iso-conversional method. The specific activation energy was calculated following a graphic method where the reaction rate plotted against temperature forms a nearly straight line over the same conversion range. Furthermore, the pre-exponential factor was extracted from consecutive plots over various heating rates using a form of the autocatalytic function. The results turn to be on the same order of magnitude with those obtained by Snegirev et al. in an experimental work on polystyrene with different molecular masses [55]. These kinetic parameters associated to the chemical reaction were further used as an input data for pyrolysis simulations performed with Fire Dynamics Simulator. The heat release rate curves generated during the simulations followed the same shape with the experimental ones, except for the graphene PS, in which case the two peaks for each chemical step are difficult to be replicated. This CFD software proved to be a reliable tool for the prediction of heat release rate, but care should be taken when Arrhenius parameters are calculated. It is always important that an optimization study to be employed in order to get accurate values of these reaction characteristics.

Although polystyrene is a thermoplastic material per se, the experimental investigation conducted with a TGA-DSC instrument revealed a particular behavior when graphite and graphene are added to its structure. Visual observations during the Cone Calorimeter experiments strengthen these findings since in both cases instead to first melt and then decompose, they started to pyrolyse first which resulted in a delay of the melting phase.

Heat release rate curves from the Cone Calorimeter measurements were then used in a qualitative study proposed to estimate the temperatures developed in a large-scale façade test in accordance to BS 8414 requirements. Samples tested in a horizontal position are intended to replicate a vertical façade fire. Due to a rapid melting of these plastic materials it is difficult to determine an accurate value for the heat release rate expected in a vertical fire. It turns out that temperatures are strongly interrelated to the heat release rate used for the simulations. Thus, it is important that a precise estimation of the input parameters in the simulation to be made. Although, temperatures generated by the fire source are well captured during the calibration and are in line with outdoor experimental studies, an accurate flame spread analysis is yet very complicated on a large-scale using CFD applications. Not only the size of the mesh it is a barrier for the flame spread simulation, but also the vertical spread of fire it is still a complex phenomenon which makes the numerical approach a hot topic among researchers.

At this moment the production of graphene is increasing and new innovative manufacturing processes are introduced on the market. Research groups are focused more and more on the development of this material which may represent a cost-effective solution for the fire

safety of the facades. Despite the fact that a cost-benefit analysis is not included in this report, the production of expanded graphene polystyrene would be similar to graphite EPS. Future work should be focused on the investigation of the reaction-to-fire class of an exterior wall assembly containing a graphene EPS insulation layer. Additionally, it should also consist in the determination of the right amount of graphene included in the polystyrene matrix, in order to achieve a balance between fire safety strategies and the cost-effectiveness of the end-use product.

To conclude, this research thesis provides a support for the development of new materials that can be included in the external systems of the building façades. Graphene integration in the polystyrene structure enhanced the flammability potential of this insulating component which may represent a viable approach in the future progress of both energy reduction and fire safety fields.

References:


1. http://www.inchem.org/documents/icsc/icsc/eics1043.htm, downloaded on 12.03.2019;
2. Yeole, N., Polystyrene-graphene oxide (GO) nanocomposite synthesized by interfacial interactions between RAFT modified GO and core-shell polymeric nanoparticles, Journal of Colloid and Interface Science, 2015;
3. Yue, L., Yuhong, Z. – Polystyrene/graphene oxide nanocomposites synthesized via Pickering polymerization, Progress in Organic Coatings, 2016;
4. Johanesson, P., Larsson, G., Fire tests with light, non-bearing external walls, Meddelande 124, Statens Provningsanstalt (SP Technical Research Institute of Sweden), 1958;
5. Ondrus, J. (1985). Fire hazards of facades with externally applied additional thermal insulation. Full scale experiments. (LUTVDG/TVBB--3021--SE; Vol. 3021). Division of Building Fire Safety and Technology, Lund Institute of Technology;
6. Yokoi S.: “Study on the Prevention of Fire Spread Caused by Hot Upward Current”, Report of the BRI, No.34, 1960;
7. Drysdale, D., An introduction to fire dynamics, Third Edition, Wiley, 2011;
8. McGuire J. H., The flammability of exterior claddings, Fire Technology 3(2):137-141, 1967;
9. Oleszkiewicz, I., Heat transfer from a window fire plume to a building façade, ASME HTD, 123, pp, 163-170, 1989;
10. Oleszkiewicz, I., Vertical separation of windows using spandrel walls and horizontal projections, Fire technology 27(4):334-340, 1991;
11. Bong, F., Fire Spread on Exterior Walls, Fire Engineering Research Report 00/1, ISSN 1173-5996, 2000;
12. Sumathipala, K., The Effect on an Interior Corner Fire on Exterior Wall Fire Spread, Poster presented at First European Symposium of Fire Safety Science, International Association of Fire Safety Science, Zurich, 1995;
13. Rogowski B. F. W., Ramaprasad R., Southern J. R., Fire performance of external thermal insulation for walls of multi-storey buildings, BRE Report 135, BRE, Fire Research Station, 1988;

14. Morris, W. A., Colwell, S., Smit, D., Andrews, A. and Connolly, R., Test Method to Assess the Fire Performance of External Cladding Systems, Fire Note 3. Fire Research Station, Building Research Establishment Ltd, 1998;
15. Colwell, S., Baker, T., Fire Performance of External Thermal Insulation for Walls of Multistorey Buildings, Third Edition, BRE Trust, BR 135, 2013;
16. Broemme, A. "Berlin: Verheerender Fassadenbrand". Deutsche Feuerwehr-Zeitung Brandschutz, August, 2005;
17. White, N., Delichatsios, M., Fire Hazards of Exterior Wall Assemblies Containing Combustible Components, Fire Protection Research Foundation, 2013;
18. https://www.nfpa.org/-/media/Files/News-and-Research/Resources/Research-Foundation/Currentprojects/PIRGprojects/ExteriorCombustibleWallsReportDraft.ashx?la=en, downloaded on 16.03.2019;
19. http://www.fire.org.uk/news/2010/11/14/seven-die-in-fire-in-immigrant-hostel-in-dijon-france.html, downloaded on 16.03.2019;;
20. http://www.fire.org.uk/news/2010/11/14/seven-die-in-fire-in-immigrant-hostel-in-dijon-france.html, downloaded on 22.03.2019;
21. https://docplayer.net/24915252-Fatal-fires-and-building-materials-how-can-we-prevent-that-more-occupants-and-fire-fighters-are-killed.html, downloaded on 18.03.2019;
22. Buletinul Pompierilor, nr. 1/2017, Editura Ministerului Afacerilor Interne, Bucharest, 2017;
23. https://sverigesradio.se/sida/artikel.aspx?programid=2054&artikel=5630338, downloaded on 12.03.2019;
24. http://safeandsustainablebuildings.com/, downloaded on 22.03.2019;
25. https://en.wikipedia.org/wiki/Exterior_insulation_finishing_system, downloaded on 12.04.2019;
26. https://www.wbdg.org/guides-specifications/building-envelope-design-guide/wall-systems/exterior-insulation-and-finish-system-eifs, downloaded on 10.02.2019;
27. https://www.terraco-eifs.com/what-is-eifs/, downloaded on 10.02.2019;
28. https://www.designingbuildings.co.uk/wiki/Metal_profile_cladding, downloaded on 18.02.2019;

29. Lamont, S., Ingolfsson, S., High Rise Buildings with Combustible Exterior Wall Assemblies: Fire Risk Assessment Tool, NFPA Research, February 2018;
30. https://www.designingbuildings.co.uk/wiki/Metal_profile_cladding, downloaded on 24.04.2019;
31. http://www.iida.org/content.cfm/exploring-the-surface-the-technical-side-of-laminate, downloaded on 16.02.2019;
32. http://www.ceicomposites.com/architecturalsystems/highpressurelaminatepanels.html, downloaded on 18.02.2019;;
33. https://www.afc.nz/high-pressure-laminate-hpl/, downloaded on 18.03.2019;
34. https://en.wikipedia.org/wiki/Structural_insulated_panel, downloaded on 18.02.2019;
35. http://www.thermasteelinc.com/product/thermasteel-composite-structural-insulated-panels, downloaded on 18.02.2019;;
36. Smith, J., The importance of rainscreen systems – Protecting your Home from Damaging Moisture, The Coastal Cottage Company, 2018;
37. Booth Muirie Limited, Architectural Cladding Systems, Coatbridge, July 2016;
38. M. J. Gollner, K. Overholt, A. S. Rangwala, J. Perricone, and F. A. Williams. Warehouse commodity classification from fundamental principles. Part I: Commodity and burning rates. Fire Safety Journal, 46(6), 2011;
39. Gollner, M., Studies on Upward Flame Spread, University of California, San Diego, 2012;
40. Rukavina, M., Carevic, M., Pecur, I., Fire Protection of Facades, The Guidelines for Designers, Architects, Engineers and Fire Experts, 2017;
41. Johnson, T., Fire and rescue Services, Dubai Civil Defence, UAE Fire Code, 2017;
42. Boström, L., Development of a European approach to assess the fire performance of facades, European Commission, Brussels, 2018;
43. Macdonald, N., A comparison of BS 8414 – 1 & 2, DRAFT din 4102-20, ISO 13785– 1 & 2, EN 13823 and ISO 11925-2, BRE Global, 2012;
44. X., Chen, Y., Liu, S., Bai, Q.. Wang, Polymer-Plastics Technology and Engineering Vol. 53, 2014;

45. Jelle, B., P., Traditional, state-of-the-art and future thermal building insulation materials and solutions – Properties, requirements and possibilities, 43(10), SINTEF, 2011;
46. https://en.wikipedia.org/wiki/Graphite, downloaded on 12.03.2019;
47. http://www.tectonicaonline.com/products/1915/modified_graphite_polystyrene_expanded_eps_neopor/, downloaded on 16.02.2019;;
48. Hosseinpour, A., Eslami, R., Kaviani, K., Esfahani, A., Effect of expandable graphite on flammability of polystyrene foams, 12th International Seminar on Polymer Science and Technology, 2016;
49. https://www.nanowerk.com/what_is_graphene.php, downloaded on 18.03.2019;
50. Chen, W., Liu, Y., Liu, P., Xu, C., Liu, Y., Wang, Q., The preparation and application of a graphene-based hybrid flame retardant containing a long-chain phosphaphenanthrene, 7:8759, 2017;
51. www.csun.edu, Experiment 1: Adiabatic Bomb Calorimeter, 2010;
52. Krupa, P, Malinaric, S., Using the Transient Plane Source Method for Measuring Thermal Parameters of Electroceramics, International Journal of Mechanical and Mechatronics Engineering, vol. 8, no. 5, 2014;
53. Flecknoe-Brown, K., W., Hostika, S., van Hees, P., Pyrolysis Modelling of Composite Fabrics Based on Individual Fabric Properties Using Micro-Combustion Calorimetry, International Conference and Exhibition on Fire Science and Engineering, 2016;
54. Lyon, R., Walters, R., Stoliarov, S., Safronova, N., Principles and Practice of Microscale Combustion Calorimetry, Federal Aviation Administration, Report DOT/FAA/TC-12/53, 2013;
55. Snegirev, A., Talalov, V., Stepanov, V., Harris, J., Formal kinetics of polymer pyrolysis for modeling of ignition and burning in fire tests, INTERFLAM, 2013;
56. SFPE Handbook of Fire Protection Engineering, Third Edition, 2002;
57. https://www.google.co.uk/search?q=cone+calorimeter+description&rlz=1C1GGRV_enGB764GB764&source=lnms&tbm=isch&sa=X&ved=0ahUKEwj7_oOn-9nXAhUIPVAKHTA6AHwQ_AUICigB&biw=1920&bih=974#imgrc=YPgiGrbxa4CekM;
58. Groenewoud, W., M., Thermogravimetry, Characterization of Polymers by Thermal Analysis, 2001;

59. BS 8414-1:2015+A1:2017 Fire performance of external cladding systems, Part 1: Test method for non loadbearing external cladding systems applied to the masonry face of a building;
60. BS 8414-2:2015+A1:2017 Fire performance of external cladding systems, Part 2: Test method for non loadbearing external cladding systems supported by a structural steel frame;
61. ISO 1716:2018 Reaction to fire tests for products – Determination of the gross heat of combustion (calorific value);
62. ISO 1928:2009 Solid mineral fuels – Determination of gross calorific value by the bomb calorimetric method and calculation of net calorific value;
63. ISO 22007-2:2015 Plastics – Determination of thermal conductivity and thermal diffusivity – Part 2: Transient plane heat source (hot disk) method;
64. ASTM 7309-11:2013 Test methods for determining flammability characteristics of plastics and other solid materials using Microscale Combustion Calorimetry;
65. Dietenberger, M., Ignitability analysis using the cone calorimeter and lift apparatus, WI 53705-2398, 1996;
66. Hjohlman, M., Andersson, P., Flame spread modeling of textile materials, SP Report 2008:34;
67. Pau, D., Fleischmann, C., Spearpoint, M., Li, K-Y., Sensitivity of heat of reaction for polyurethane foams, Fire Safety Science Proceedings, IAFFS, 2014;
68. MOHAN, A., T., Simulation of Pyrolysis in Fire Dynamics Simulator (FDS), Cantene, 2018;
69. http://www.chimneykings.com/hazard-detail-pyrolysis.html, downloaded on 12.03.2019;
70. KIM, M., E., Parameter Estimation Methods for Comprehensive Pyrolysis Modeling, Worcester Polytechnic Institute, 2014;
71. McGrattan, K., Hostikka, S., McDermott, R., Floyd, J., Weinschenk, C., Overholt, K., Fire Dynamics Simulator Technical reference Guide Volume 1: Mathematical Model, Sixth Edition, 2013;
72. Bjegovic, D., Pecur, I., Milovanovic, B., Rukavina, M., Bagaric, M., Comparative full-scale fire performance testing of ETICS systems, Gradevinar, 5/2016;

73. Anderson, J., Bostrom, L., Jansson, R., Fire Safety of Facades, SP Report 2017:37, RISE, Sweden, 2017;
74. McGrattan, K., McDermott, R., Weinschenk, C., Overholt, K., Fire Dynamics Simulator User's Guide, NIST Special Publication 1019, Sixth Edition, 2013;
75. Bao, C., Song, L., Wilkie, C., Yuan, B., Guo, Y., Hu, Y., Gong, X., Graphite oxide, graphene, and metal-loaded graphene for fire safety applications of polystyrene, Journal of Materials Chemistry, 2012;
76. SP Fire Technology, "SP Fire 105, External wall assemblies and facade claddings: Reaction to fire", Issue No: 5, SP Technical Research Institute of Sweden, Borås, 1994;
77. Patrick van Hees, Development of full-scale façade tests in ISO TC92, MATEC Web of Conferences 46, 2016.

## Appendix 1: TGA-DSC results

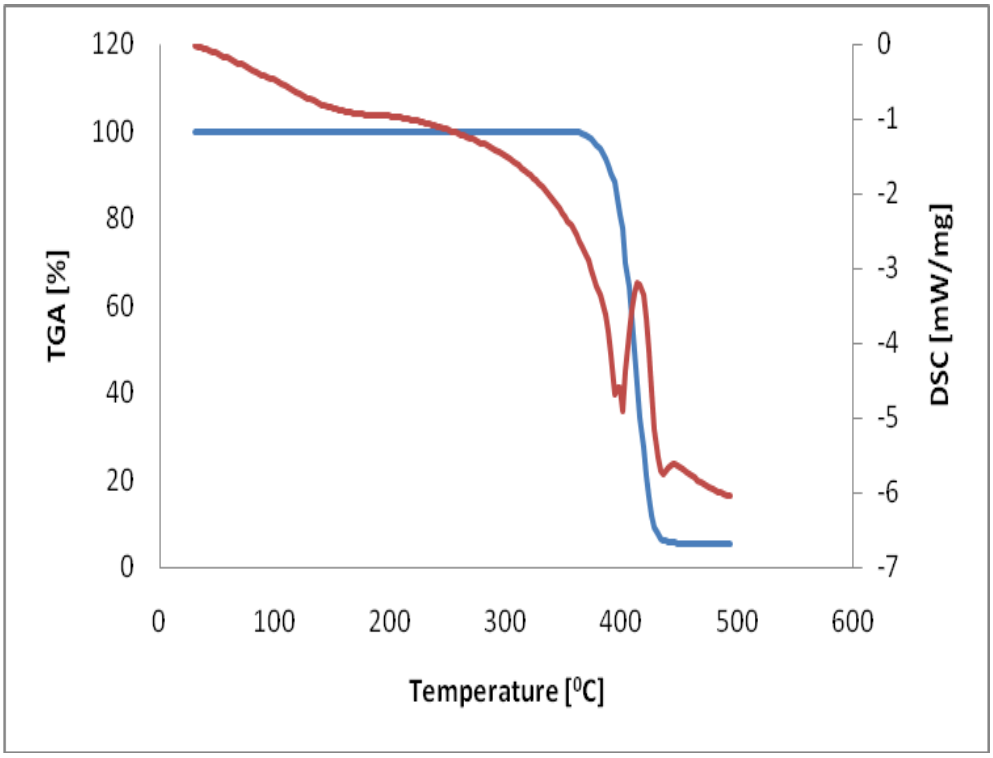


Figure 52. TGA and DSC curves for graphene PS

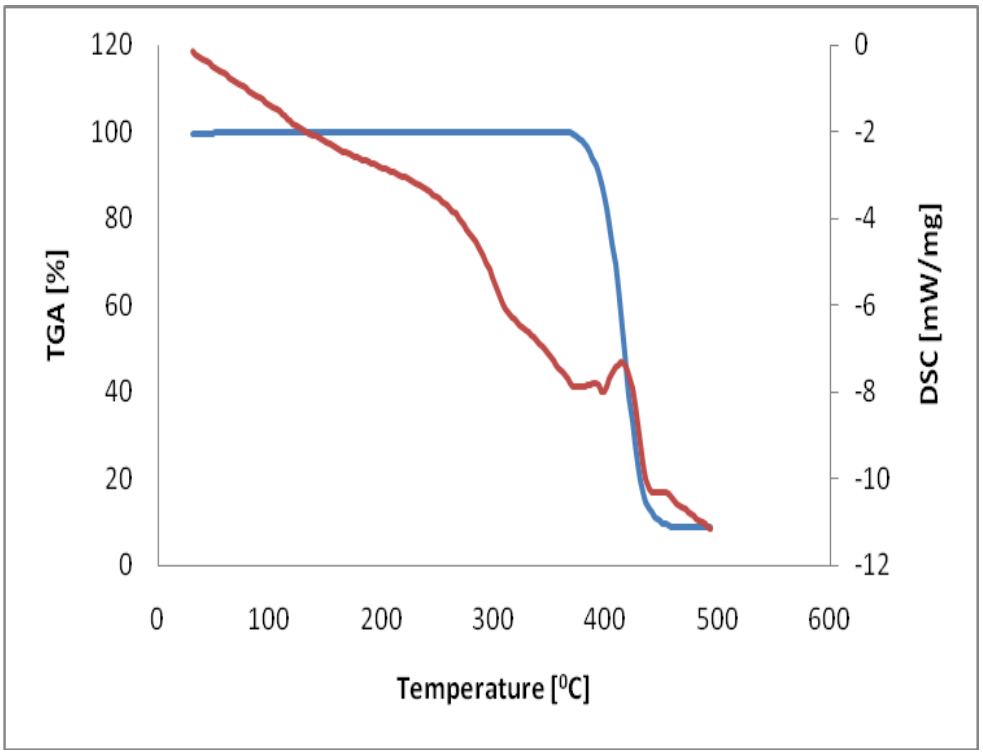


Figure 53 TGA and DSC curves for graphite EPS

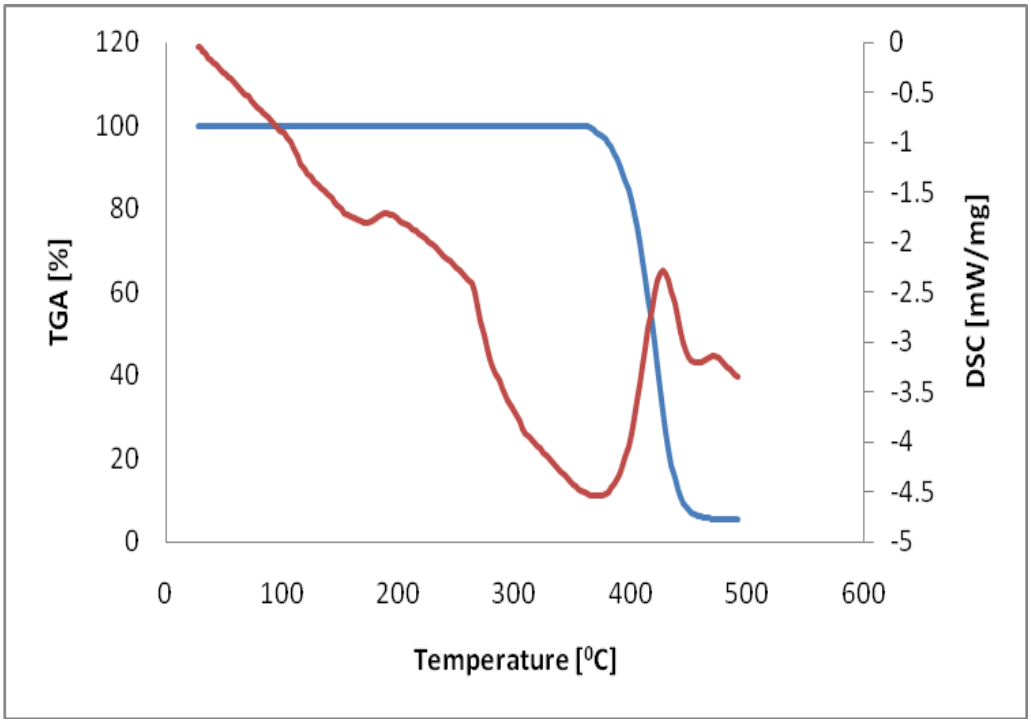


Figure 54 TGA and DSC curves for high density EPS

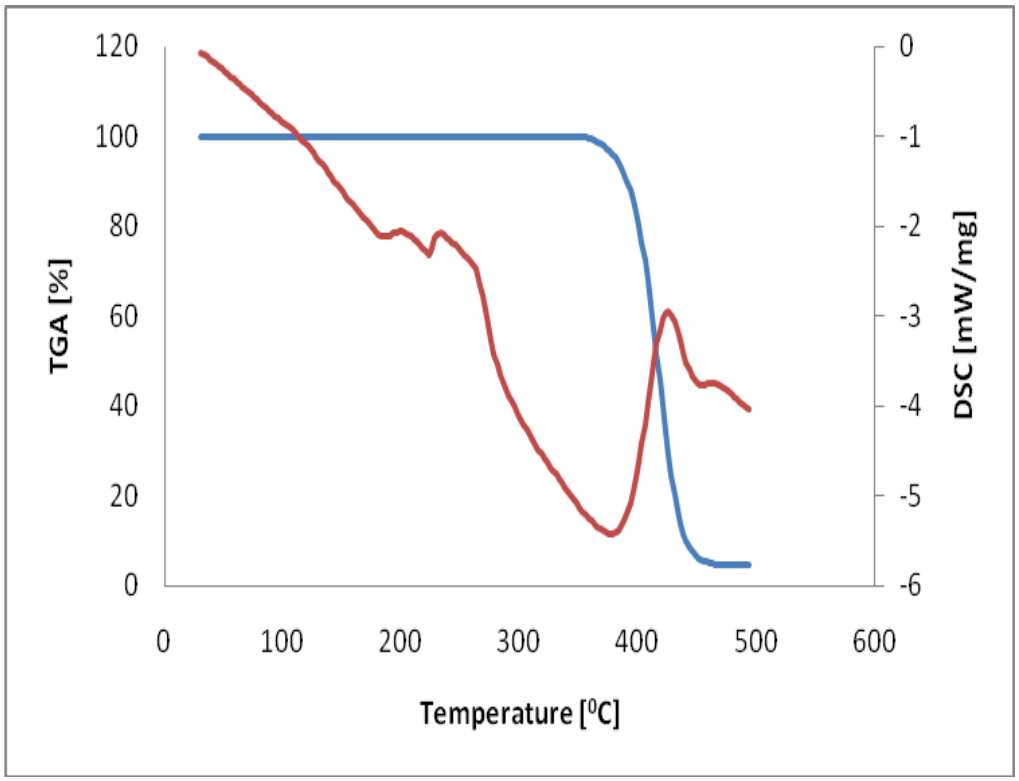


Figure 55 TGA and DSC curves for low density EPS

## Appendix 2: MCC comparative results

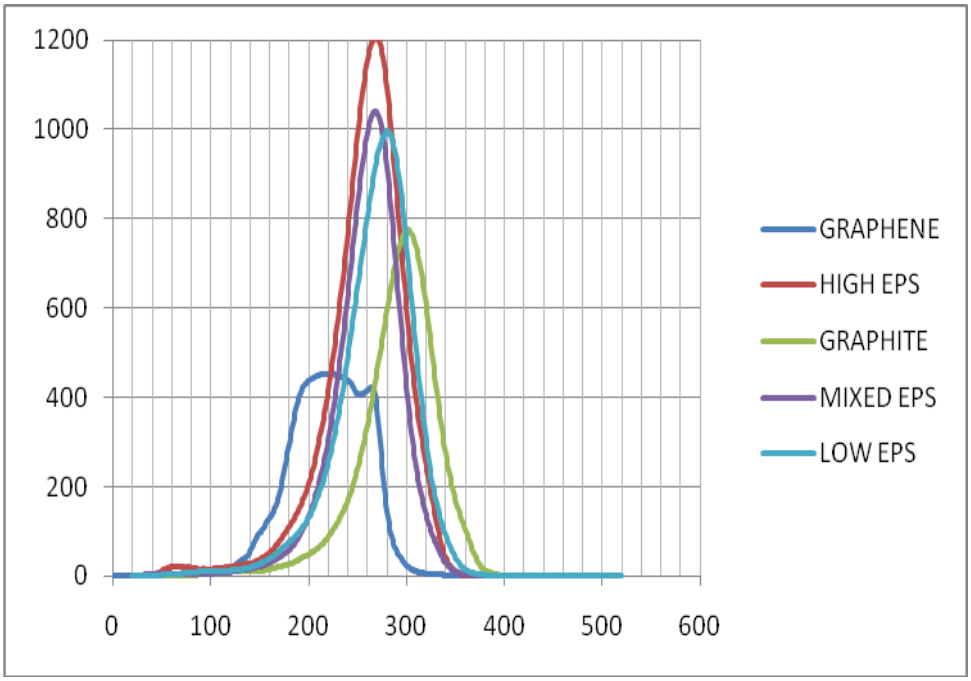


Figure 56 Heat release rate profiles on a $80^0$ C/min heating rate

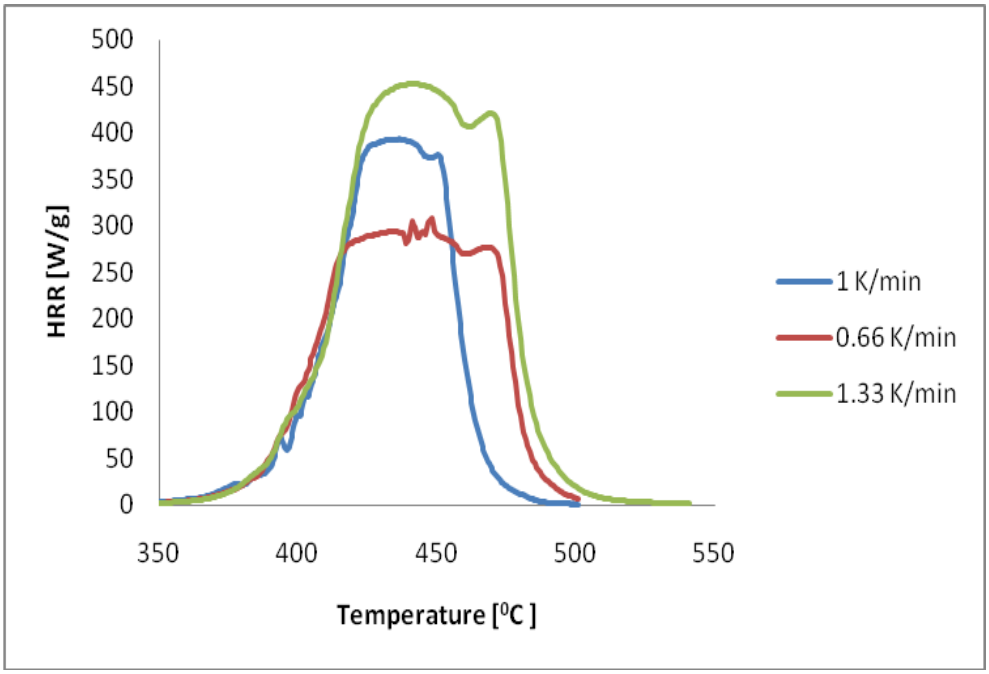


Figure 57 Heat release rate profiles for graphene PS at different heating rates

## Appendix 3: FDS code for MCC numerical simulation of low density EPS

```
&HEAD CHID='EPS_MCC', TITLE='MCC numerical simulation' /

&MESH IJK=3,1,4, XB=-2,2,-0.5,0.5,0,1 /

&MISC SOLID_PHASE_ONLY =.TRUE./

&TIME T_END=1000. /

&REAC FUEL='PROPANE', HEAT_OF_COMBUSTION = 33271.0/

&VENT XB=-1,1,-0.5,0.5,0.0,0.0, SURF_ID='SAMPLE' /

&SURF ID = 'SAMPLE'
TGA_ANALYSIS = .TRUE.
TGA_HEATING_RATE = 60.0
TGA_FINAL_TEMPERATURE = 900.0
COLOR = 'RED'
THICKNESS = 0.1
MATL_ID(1,1) = 'component 1'
MATL_MASS_FRACTION(1,1) = 1.0/

&MATL ID = 'component 1'
EMISSIVITY = 0.81
DENSITY = 15.
CONDUCTIVITY = 0.03
SPECIFIC_HEAT = 1.11
N_REACTIONS = 1
REFERENCE_TEMPERATURE = 441.49
REFERENCE_RANGE = 0.022182
HEATING_RATE = 60.0
NU_SPEC = 0.98
SPEC_ID = 'PROPANE'
NU_MATL = 0.02
MATL_ID = 'residue'/

&MATL ID = 'residue'
DENSITY = 5.
CONDUCTIVITY = 0.03
SPECIFIC_HEAT = 1.11 /

&TAIL /
```

## Appendix 4: FDS temperature results for large-scale model on the lateral wing of the rig

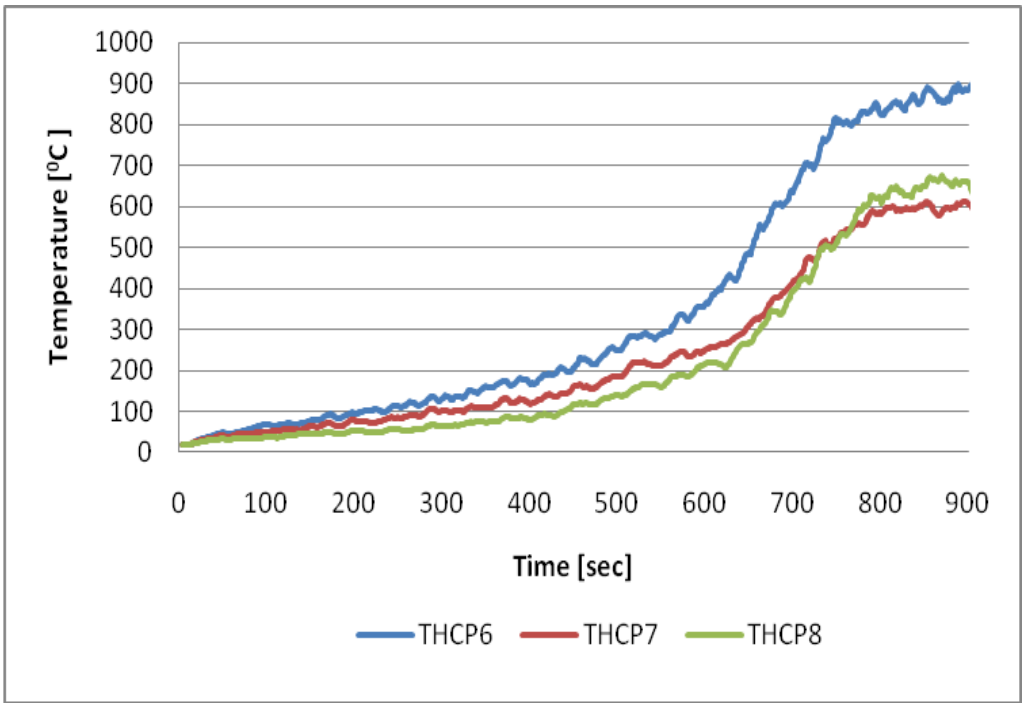


Figure 58 Temperature values at first level on the right wing for low density EPS

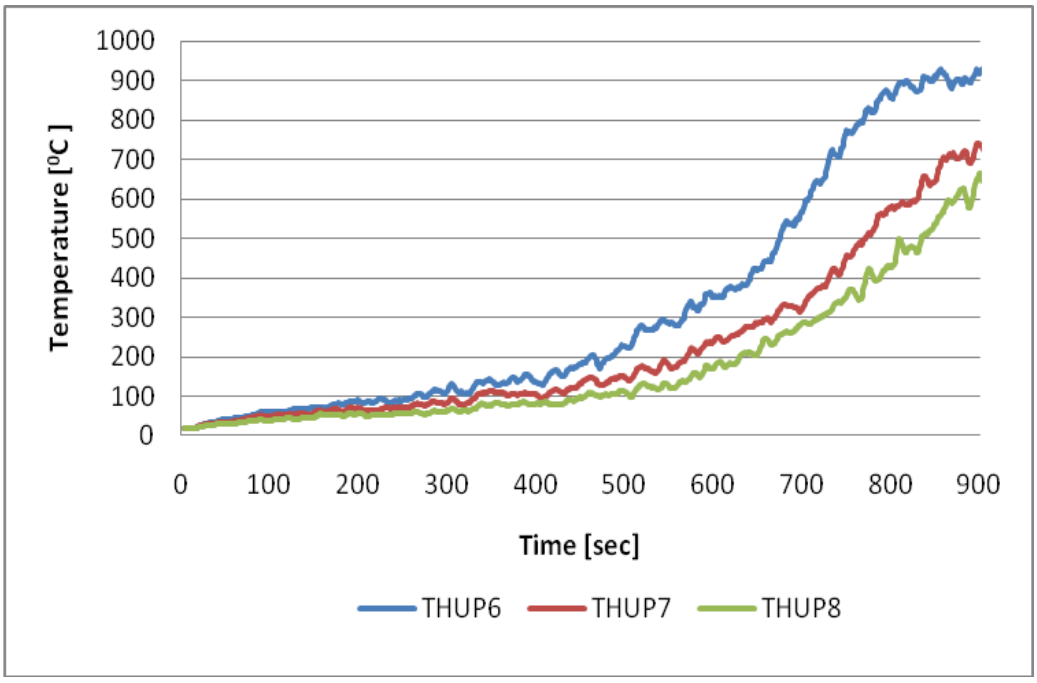


Figure 59 Temperature values at second level on the right wing for low density EPS

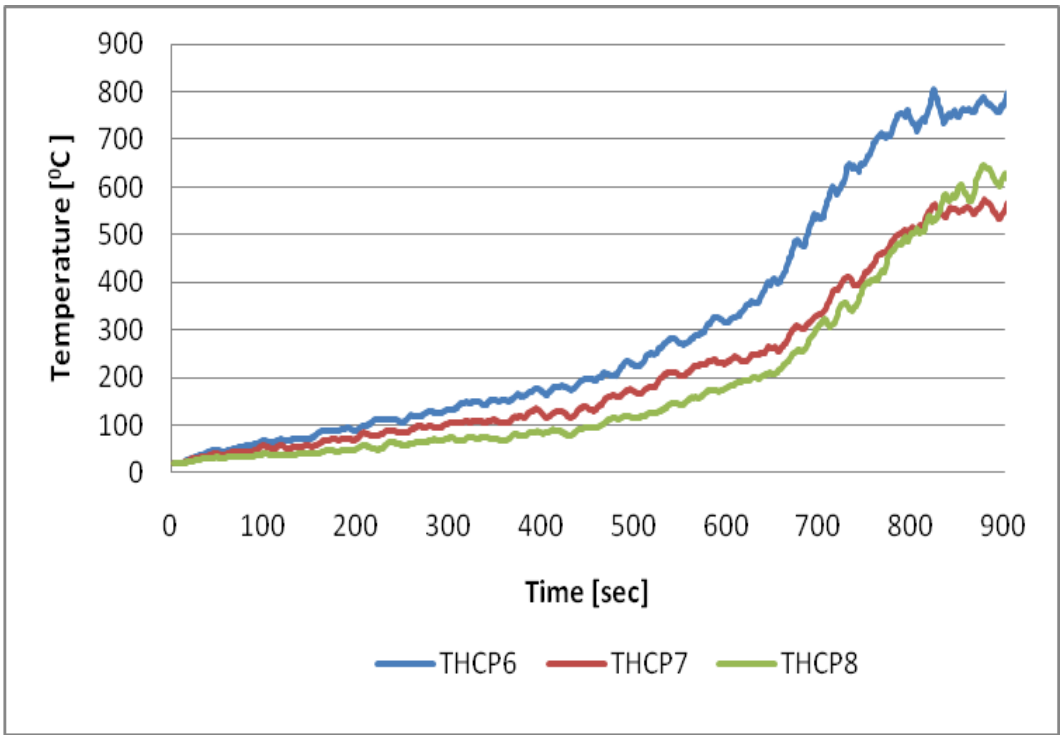


Figure 60 Temperature values at first level on the right wing for graphene PS

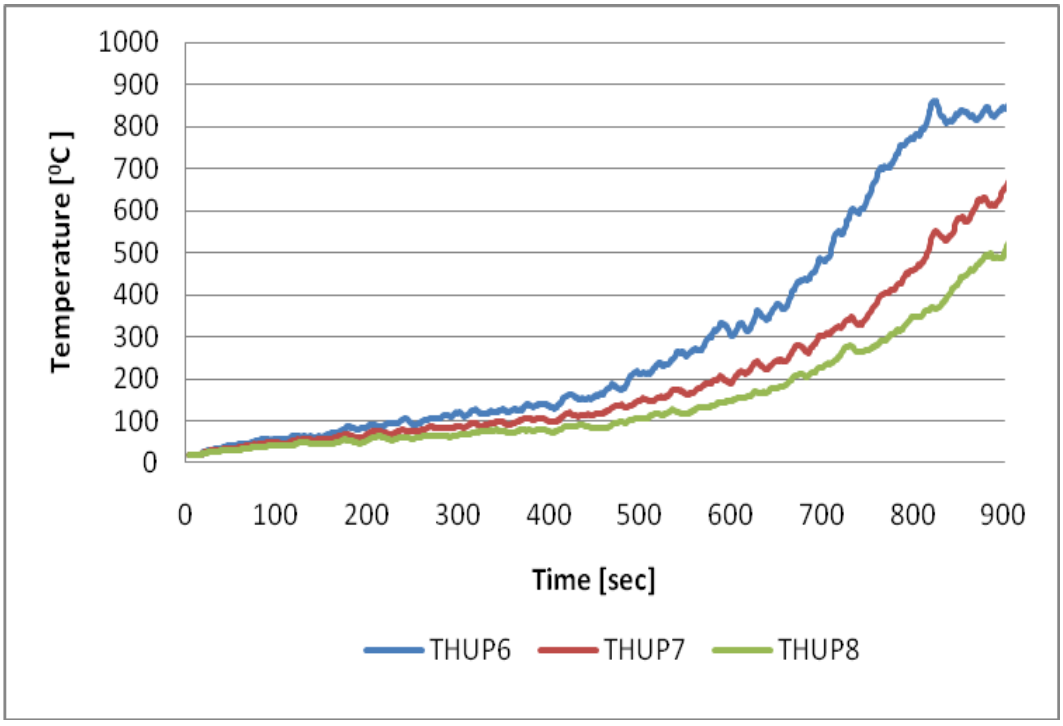


Figure 61. Temperature values at second level on the right wing for graphene PS